Chaos, Solitons and Fractals 186 (2024) 115295

Contents lists available at ScienceDirect

Chaos, Solitons and Fractals

journal homepage: www.elsevier.com/locate/chaos

Understanding the dual effects of linear cross-diffusion and geometry on reaction–diffusion systems for pattern formation

Wakil Sarfaraz [a], Gulsemay Yigit [b], Raquel Barreira [c,d], Lakhdar Remaki [e], Muflih Alhazmi [f], Anotida Madzvamuse [g,h,i,j,*]

[a] Professional Development Expert (PDE), Corndel Ltd., 410 Highgate Studio 53-79 Highgate Road, London NW5 1TL, United Kingdom
[b] Department of Mathematics, Faculty of Engineering and Natural Sciences, Bahcesehir University, Istanbul, Turkey
[c] Instituto Politécnico de Setúbal, Escola Superior de Tecnologia do Barreiro, Rua Américo da Silva Marinho-Lavradio 2839-001 Barreiro, Portugal
[d] Centro de Matemática, Aplicações Fundamentais e Investigação Operacional (CMAFcIO), Universidade de Lisboa, Portugal
[e] Department of Mathematics and Computer Science, Alfaisal University, P.O. Box 50927, Riyadh 11533, Saudi Arabia
[f] Mathematics Department, Faculty of Science, Northern Border University, Arar, Saudi Arabia
[g] Mathematics Department, The University of British Columbia, Mathematics Building, 1984 Mathematics Road, Vancouver, BC Canada V6T 1Z2
[h] Department of Mathematics and Applied Mathematics, University of Pretoria, Pretoria 0132, South Africa
[i] Department of Mathematics and Applied Mathematics, University of Johannesburg, PO Box 524 Auckland Park, 2006, South Africa
[j] Department of Mathematics and Computational Sciences, University of Zimbabwe, Mt Pleasant, Harare, Zimbabwe

ARTICLE INFO

Keywords:
Reaction–diffusion systems
Pattern formation
Diffusion-driven instability
Cross-diffusion
Turing instability
Domain-dependency
Hopf and transcritical bifurcations

ABSTRACT

In this work, we study the dual effects of linear cross-diffusion and geometry on reaction–diffusion systems for pattern formation on rectangular domains. The spatiotemporal dynamics of the reaction–diffusion system with linear cross-diffusion are explored for the case of an activator-depleted model of two chemical species in terms of the domain size and its model parameters. Linear stability analysis is employed to derive the constraints which are necessary in understanding the dual roles of linear cross-diffusion and domain-size in studying the instability of the reaction–diffusion system. The conditions are proven in terms of lower and upper bounds of the domain-size together with the reaction, self- and cross-diffusion coefficients. The full parameter classification of the model system is presented in terms of the relationship between the domain size and cross-diffusion-driven instability. Subsequently, regions showing Turing instability, Hopf and transcritical types of bifurcations are demonstrated using the parameter values of the system. In this work, our theoretical findings are validated according to the proper choice of parameters in order to understand the effects of domain-size and linear cross-diffusion on the long-term spatiotemporal behaviour of solutions of the reaction–diffusion system. For illustrative purposes, numerical simulations showing each of the three types of dynamics are examined for the Schnakenberg kinetics, also known as an activator-depleted reaction kinetics.

1. Introduction

Reaction–diffusion systems (RDSs) have been extensively studied as a class of the prominent models for investigating the pattern generation in various biological and chemical processes [1–8]. The evolution of self-organising pattern formation was introduced by Alan Turing in his seminal work [9] through a detailed justification of how and why reaction–diffusion systems could explain the dynamics of chemical morphogenesis that are responsible for the emergence of pattern formation in nature. Activator-depleted reaction kinetics known as Schnakenberg kinetics [1,3,7,10] modelled with diffusive systems, is one of the well-known reaction kinetics for investigating the spatiotemporal dynamics of patterns induced by the reaction–diffusion theory.

Diffusion processes can be characterised in a variety of forms in many multi-component systems. One of these forms of diffusion is cross diffusion, which serves to explain a process in which a gradient in concentration of one chemical or biological species induces the fluxes of another species [4]. The classical pattern formation mechanism in reaction–diffusion systems in the absence of cross-diffusion requires the existence of long-range inhibition and short-range activation, which implies that the diffusion coefficient of the inhibitor should be significantly greater than the diffusion coefficient of the activator [3,7]. On the other hand, the existence of cross-diffusion enables the usage of equal rates of diffusion coefficients. It has been shown that the

* Corresponding author at: Mathematics Department, The University of British Columbia, Mathematics Building, 1984 Mathematics Road, Vancouver, BC Canada V6T 1Z2 .
E-mail address: am823@math.ubc.ca (A. Madzvamuse).

https://doi.org/10.1016/j.chaos.2024.115295
Received 9 January 2024; Received in revised form 17 June 2024; Accepted 13 July 2024
Available online 23 July 2024

presence of cross-diffusion in RDSs has a significant and positive effect on the ability of reaction–diffusion systems to form patterns [4,7,8,11]. Cross-diffusive induced pattern formation has been extensively studied in several biochemical applications such as interactions of solutes [4, 12,13], prey-predator systems [14–16], chemotaxis [17,18]. A study in [19] focused on the generation of different kind of bifurcation regions for the cross diffusive RDS to exhibit pattern formation. Turing instability analysis have been discussed in [7,8] with the necessary conditions for such systems to exhibit pattern formation on stationary and growing domains, respectively.

Linear stability analysis is a useful tool to investigate stability and instability conditions for the spatiotemporal dynamics of RDS around a uniform steady state. These conditions are determined by the eigenvalues of the linearised time-dependent stability matrix. With the linear stability analysis, regions corresponding to pattern formation can be created in the presence of self or cross-diffusion [7,20–22]. Parameter classification has a significant importance in the analysis of the mechanisms for pattern formation formulated by RDSs. The works presented in [7,8], provide a detailed linear stability analysis, which is proposed with the derivation of the necessary conditions for the cross-diffusive system to exhibit Turing instability on static and evolving domains respectively. The study in [7,8] focused mainly on finding the unstable regions of parameter spaces confined only to Turing diffusion-driven instability in the presence of cross-diffusion for the activator-depleted model. One of the novelty of this study is to derive sufficient conditions relating the domain-size to the necessary cross-diffusion driven instability conditions proposed in [7,8]. The methodology used in the current work compared to [7,8] is completely independent i.e. a dynamical system's approach utilising the spectrum of the Laplace operator in classifying the parameter spaces is novel. The classification of the parameter spaces in the current study is not only limited to the Turing spaces (which is the case in [7,8]). Moreover, the current study extends to acquire a full classification of the admissible parameter spaces of the RDSs, which entails the regions pertinent to different dynamical properties such as spatial and spatiotemporal pattern formation. The numerical simulations in the current manuscript successfully demonstrate a diverse set of dynamical properties (spatial and spatiotemporal) of the Schankenberg RDS. While demonstrating our key results, it turns out that the results of [7,8] form a subset of the generalised spatiotemporal dynamical properties discovered in the current study. For a traditional RDS to undergo the mechanism of pattern formation, it is shown in [1,9,23] that the domain must satisfy a critical scale. The work in this article extends the analysis of domain size to explore beyond the necessary conditions for diffusion-driven instability and to discover the effects of domain size and linear cross-diffusion on the dynamical properties of RDSs.

Studies in the field of RDSs have shown that bifurcation analysis plays an important role in understanding the spatiotemporal dynamical characteristics of the system near a uniform steady-state [24–32]. Recently, more attention has been paid in bifurcation analysis for the prey-predator RDs with and without cross diffusion [33–36]. However, in most current state-of-the-art studies, there is still a lack of explanation on the relationship (and its role) between the domain size and different bifurcation types. A study conducted in [22] addressed the full classification of parameter spaces in the combination of spatial pattern and temporal periodicity on rectangular domains without cross-diffusion. Hence, this study substantially extends these results by taking into account cross-diffusion to relate the domain size and the system parameter values in the presence of linear cross-diffusion. The domain-dependent analysis is highly dependent on the problem geometry. A recent study in [37] addressed a quantitative analysis on the relation between the domain-size of domain and spatiotemporal analysis of cross-diffusive reaction–diffusion systems on circular domains. In contrast, theoretical analysis of this paper is explicitly articulated with a focus on flat rectangular domains, with simpler eigenfunctions rather than the complex Bessel functions which arise on circular domains, thereby exhibiting a clear distinction in the presentation of results between these distinct geometric contexts. We provide rigorous analysis, parameter spaces on which other researchers can use to study these models and the exhibition of patterns formed under the theoretical findings. In order to validate our theoretical findings, a state-of-the-art finite element method is applied to provide approximate numerical solutions.

Many of the RDSs contain nonlinear terms which makes them impractical to obtain closed-form solutions. This difficulty can be overcome by using suitable computational approaches. Therefore, it becomes attractive to explore numerical methods to understand the dynamical behaviour of RDSs. It has been well demonstrated in the literature that the finite element method is one of the powerful numerical method for the spatial discretisation of RDSs [38–43]. According to this procedure, the system of partial differential equations is first discretised in space using the finite element method which produces a time-dependent system of ordinary differential equations (ODEs), followed by the time discretisation using several time-stepping schemes to obtain the desired numerical solution [44]. On the other hand, classification of the parameter space plays a fundamental role in the parameter selection during the numerical discretisation process. In this work, our theoretical findings have been validated according to the proper choice of parameters in order to understand the spatiotemporal dynamics of the reaction–diffusion system in the presence of linear cross-diffusion.

In this work, we aim to classify the domain-dependent parametrisation and distinguish between the temporal bifurcation and spatial instability in the presence of linear cross-diffusion using the well-known activator-depleted model of two chemical species. This process includes the linear stability analysis of the interaction of these two species in terms of domain size and the influence of cross-diffusion. We use linear stability analysis to derive the constraints on the domain-size, necessary to understand the role of linear cross-diffusion in driving the diffusion-driven instability of the system. Relating the domain-size and linear cross-diffusion driven system parameter values enables us to present the full parameter spaces. Analytical results are verified and supported by finite element solutions of the full reaction–diffusion system with linear cross-diffusion.

Hence, the novelty and key contributions of our work to current-state-of-the-art literature on reaction–diffusion systems for pattern formation is the dual interplay between linear cross-diffusion and the domain-length. In our study, domain-length acts as a bifurcation parameter which characterises the transition of solution behaviour from Turing, Hopf and transcritical bifurcations. By introducing linear cross-diffusion, the conditions for diffusion-driven instability are substantially relaxed. In particular, equal self-diffusion coefficients can give rise to pattern formation only in the presence of linear cross-diffusion. Moreover, we have derived sufficient conditions relating the domain-size to the necessary and sufficient conditions for cross-diffusion driven instability. Unlike previous studies which focused on understanding only Turing cross-diffusion-driven instability, in this work, we have substantially extended these results to study conditions under which domain-size coupled with linear cross-diffusion drive Turing instability, Hopf and transcritical bifurcations.

Hence, this article is organised as follows. In the following section, we present the cross-diffusive reaction–diffusion model with its related initial and boundary conditions on a rectangular domain. In Section 2, we present the linear stability analysis performed around a uniform steady state using Taylor's theorem in two variables. In this section, we also present the necessary and sufficient conditions for the system to exhibit Turing instability, Hopf bifurcation, and limit cycle behaviour. Section 3 presents numerical generation of the parameter spaces to show the effect of self- and cross-diffusion processes on the dynamics of the system. Section 4 presents finite element solutions of the cross-diffusive reaction–diffusion system. Finally, in Section 5, we discuss the novelty of our findings and propose directions of future work.

1.1. Model equations

The non-dimensionalised form of the RDs in the presence of linear cross-diffusion for two chemical species $u(x, y, t)$ and $v(x, y, t)$ with homogeneous Neumann boundary conditions reads as

$$\begin{cases} \dfrac{\partial u}{\partial t} = \Delta u + d_v \Delta v + \gamma f(u, v),\ (x, y) \in \Omega, t > 0 \\ \dfrac{\partial v}{\partial t} = d\,\Delta v + d_u \Delta u + \gamma g(u, v) \\ \mathbf{n} \cdot \nabla u = \mathbf{n} \cdot \nabla v = 0,\ (x, y) \in \partial\Omega,\ t \geq 0 \\ u(x, y, 0) = u_0(x, y),\ \ v(x, y, 0) = v_0(x, y), \\ \quad (x, y) \in \partial\Omega,\ \ t = 0. \end{cases} \tag{1}$$

System (1) is considered on a bounded planar domain Ω, where the positive constants d and γ represent the non-dimensional diffusion and reaction coefficients respectively. The outward normal unit vector to the boundary $\partial\Omega$ is denoted by $\mathbf{n}$. The non-dimensional coefficients for self and linear cross-diffusion are respectively defined in terms of the dimensional coefficients as $d = \frac{D_v}{D_u}$, $d_u = \frac{D_{uv}}{D_u}$, and $d_v = \frac{D_{vu}}{D_u}$ (see [7,8] for further details). The functions $f(u, v) = \alpha - u + u^2 v$ and $g(u, v) = \beta - u^2 v$, represent the nonlinear [7,8] coupling reaction kinetics with positive constants α and β. The system is subject to zero-flux boundary conditions and strictly positive spatial initial conditions u_0 and v_0.

Remark. The rectangular region is considered as $\Omega = [0, L_x] \times [0, L_y]$ where L_x and L_y denotes the side lengths of the area. For practical purposes, we consider $L_x = L_y$, which means the area of the domain is taken as L^2 [22].

1.1.1. Well-posedness and global existence and uniqueness of solutions

In order for system (1) to be well-posed, the normally elliptic condition for semi-linear parabolic partial differential equations must be satisfied (an interested reader is referred to see [45–47] for further details). To view the condition more clearly, it is better to write system (1) in matrix–vector form as follows

$$\mathbf{U}_t = \mathbf{D}\Delta\mathbf{U} + \gamma\mathbf{F}(\mathbf{U}), \tag{2}$$

with appropriate initial and boundary conditions. Here,

$$\mathbf{U} = \begin{pmatrix} u \\ v \end{pmatrix},\ \mathbf{D} = \begin{pmatrix} 1 & d_v \\ d_u & d \end{pmatrix},\ \text{and}\ \mathbf{F} = \begin{pmatrix} f(u, v) \\ g(u, v) \end{pmatrix}.$$

The so-called normally elliptic condition on the diffusion parameters d, d_u and d_v requires that the diffusion tensor matrix $\mathbf{D}$ is positive definite and that entails that $d - d_u d_v > 0$. This regularity condition ensures the well-posedness of the system of partial differential equations [45–47]. This elliptic condition also ensures the global existence and uniqueness of solutions for the full nonlinear system, provided the reaction-kinetics given by $\mathbf{F}$ are Lipschitz continuous or that they satisfy maximum principles (see [47], Chapter 14). For details, on classical global existence and uniqueness of solutions of reaction–diffusion in the absence of cross-diffusion, see the work of [47], Chapter 14. The proof of the global existence and uniqueness of the solutions for System (2) in the presence of linear cross-diffusion should follow similar arguments, however, this is not a trivial calculation.

It must be noted that the analysis for global existence and uniqueness of solutions of reaction–diffusion systems on growing domains was carried out in [48], only in the presence of self-diffusion. The results hold true in the absence of domain growth. However, the inclusion of cross-diffusion both in the absence and presence of domain growth has not yet been carried and this remains an open problem.

2. Stability analysis in the presence of linear cross-diffusion

System (1) admits a constant uniform steady state solution given by $(u_s, v_s) = (\alpha + \beta, \frac{\beta}{(\alpha+\beta)^2})$ [7,8,22]. This steady state is a unique stationary point which is a solution to the system of nonlinear algebraic equations given by the reaction kinetics i.e. $f(u_s, v_s) = g(u_s, v_s) = 0$, and the zero-flux boundary conditions enforced on System (1). We proceed with the conventional application of linear stability theory to locally perturb System (1), and thereby investigate the local evolution of the dynamics of the perturbed variables namely $(u, v) = (u_s + \epsilon\bar{u}, v_s + \epsilon\bar{v})$ in the neighbourhood of the uniform steady state, $\epsilon \ll 1$. The perturbation variables $(\bar{u}, \bar{v})$ are assumed sufficiently smooth to satisfy the conditions for Taylor expansion on functions of two variables leading to the derivation of a linearised approximation of System (1) neglecting $O(\epsilon^2)$ and higher order terms, which in the matrix–vector notation is given by,

$$\frac{\partial\bar{\mathbf{w}}}{\partial t} = \mathbf{D}\Delta\bar{\mathbf{w}} + \gamma\mathbf{J}_\mathbf{F}\bar{\mathbf{w}} \tag{3}$$

where $\bar{\mathbf{w}}$, $\mathbf{D}$, $\mathbf{F}$, and the Jacobian matrix $\mathbf{J}_\mathbf{F}$ are respectively expressed as

$$\bar{\mathbf{w}} = \begin{bmatrix} \bar{u} \\ \bar{v} \end{bmatrix},\ \mathbf{D} = \begin{bmatrix} 1 & d_v \\ d_u & d \end{bmatrix},\ \mathbf{F}(u, v) = \begin{bmatrix} f(u_s, v_s) \\ g(u_s, v_s) \end{bmatrix},$$

and

$$\mathbf{J}_\mathbf{F} = \begin{bmatrix} f_u(u_s, v_s) & f_v(u_s, v_s) \\ g_u(u_s, v_s) & g_v(u_s, v_s) \end{bmatrix}. \tag{4}$$

The linearisation procedure is completed by finding the eigenfunctions of the Laplace operator satisfying the homogeneous Neumann boundary conditions. Without loss of generality the eigen-expansion of $\bar{u}$ and $\bar{v}$ for the spectrum of the Laplace operator on planar rectangular domains is assumed to hold a similar form. With this in mind the corresponding eigenvalue problem is given by

$$\begin{cases} \dfrac{\partial^2\bar{u}}{\partial x^2} + \dfrac{\partial^2\bar{u}}{\partial y^2} = k^2\bar{u}, & (x, y) \in \Omega, \\ \dfrac{\partial\bar{u}}{\partial x} = \dfrac{\partial\bar{u}}{\partial y} = 0 & (x, y) \in \partial\Omega, \end{cases} \tag{5}$$

where k determines the mode of the eigenfunctions satisfying Eq. (5).

Using the standard method of separation of variables the eigenvalue problem (5) on Ω satisfies a closed form infinite paired series of orthogonal functions and discrete positive eigenvalues in the form $(\bar{u}_{n,m}, k^2)$, which are expressed as

$$\bar{u}_{n,m}(x, y) = \sum_{n=0}^{\infty}\sum_{m=0}^{\infty} U_{n,m}\cos\Big(\frac{n\pi x}{L}\Big)\cos\Big(\frac{m\pi y}{L}\Big), \tag{6}$$

where m, n are natural numbers, i.e. $m, n \in \mathbb{N}$. In (6), $U_{n,m}$ represents the mode dependent coefficients of the eigen-expansion of the series solution to (5). The solution of System (1) is written as a separable ansatz consisting of infinite expansion of the product of an exponential decay in the time variable t and the spectrum of the two-dimensional Laplace operator for the space variables x and y, which leads to writing

$$\begin{aligned} \bar{u}(x, y, t) &= \sum_{n=0}^{\infty}\sum_{m=0}^{\infty} U_{n,m}\exp(-k_{n,m}^2 t)\cos\Big(\frac{n\pi x}{L}\Big)\cos\Big(\frac{m\pi y}{L}\Big), \\ \bar{v}(x, y, t) &= \sum_{n=0}^{\infty}\sum_{m=0}^{\infty} V_{n,m}\exp(-k_{n,m}^2 t)\cos\Big(\frac{n\pi x}{L}\Big)\cos\Big(\frac{m\pi y}{L}\Big), \end{aligned} \tag{7}$$

where $U_{n,m}$ and $V_{n,m}$ represent the unknown coefficients of the series solution. Here, we have defined

$$k^2 := k_{n,m}^2 = \frac{(m^2 + n^2)\pi^2}{L^2}. \tag{8}$$

Substituting solution (7) into system (1) leads to a fully linearised dynamical system of ODEs

$$\begin{bmatrix} \bar{u}_t \\ \bar{v}_t \end{bmatrix} = \begin{bmatrix} -k^2 + \gamma f_u & -d_v k^2 + \gamma f_v \\ -d_u k^2 + \gamma g_u & -d k^2 + \gamma g_v \end{bmatrix} \begin{bmatrix} \bar{u} \\ \bar{v} \end{bmatrix}, \tag{9}$$

where the partial derivatives are evaluated at the uniform steady state (u_s, v_s).

The components of the matrix on the right hand-side of (9) are explicitly found in terms of the system parameters using the partial derivatives of the reaction kinetics $f(u,v)$ and $g(u,v)$. These are evaluated at the uniform steady state solutions (u_s, v_s), which leads to writing the two-component dynamical system (9) in the form of a two-dimensional discrete eigenvalue problem given by

$$\begin{bmatrix} \gamma\frac{\beta-\alpha}{\alpha+\beta} - k^2 & \gamma(\beta+\alpha^2) - d_v k^2 \\ -\gamma\frac{2\beta}{\alpha+\beta} - d_u k^2 & -\gamma(\beta+\alpha^2) - dk^2 \end{bmatrix} \begin{bmatrix} \bar{u} \\ \bar{v} \end{bmatrix} = \lambda \begin{bmatrix} \bar{u} \\ \bar{v} \end{bmatrix}. \tag{10}$$

Solving (10) for λ requires to find the roots of the corresponding characteristic polynomial, which in terms of the trace and determinant of the stability matrix on the left hand-side of (10) is a quadratic equation in λ of the form

$$\lambda^2 - \mathcal{T}(\alpha,\beta)\lambda + D(\alpha,\beta) = 0. \tag{11}$$

Hence, the eigenvalues are the roots of (11), which are given by

$$\lambda_{1,2} = \frac{\mathcal{T}(\alpha,\beta) \mp \sqrt{\mathcal{T}^2(\alpha,\beta) - 4D(\alpha,\beta)}}{2}, \tag{12}$$

where $\mathcal{T}(\alpha,\beta)$ and $D(\alpha,\beta)$ denote the trace and determinant, respectively expressed in terms of the system parameters as

$$\mathcal{T}(\alpha,\beta) = \gamma\left(\frac{\beta-\alpha}{\alpha+\beta} - (\beta+\alpha)^2\right) - (d+1)k^2 \tag{13}$$

and

$$\begin{aligned} D(\alpha,\beta) = &\left(\gamma\frac{\beta-\alpha}{\alpha+\beta} - k^2\right)\left(-\gamma(\beta+\alpha)^2 - dk^2\right) \\ &-\left(\gamma(\beta+\alpha)^2 - d_v k^2\right)\left(-\gamma(\frac{-2\beta}{\alpha+\beta}) - d_u k^2\right). \end{aligned} \tag{14}$$

Note that in addition to depending on d and γ, the roots given by (12) now depend also on the cross-diffusion coefficients namely d_u and d_v. The influence of such dependence of $\mathcal{T}(\alpha,\beta)$ and $D(\alpha,\beta)$ on cross-diffusion coefficients is thoroughly investigated and, in addition to the necessary conditions proposed in [7], a set of sufficient conditions are derived and presented in the form critical inequalities imposed on the domain-size controlling parameter L to determine the dynamical properties of pattern formation modelled by (1). To verify the analytical findings due to the influence of cross-diffusion coefficients, we demonstrate by numerical computations that sub-regions for the proposed dynamics of pattern formation exist within the admissible parameters spaces $(\alpha,\beta) \in \mathbb{R}^2_+$.

2.1. Analysis for spatiotemporal pattern formation

We first analyse the characteristic polynomial (11), when the roots are a pair of complex conjugate values. Note that the admissible parameter spaces are partitioned by a curve satisfying the equation

$$\mathcal{T}^2(\alpha,\beta) - 4D(\alpha,\beta) = 0, \tag{15}$$

one side of which corresponds to $\lambda_{1,2} \in \mathbb{R}$ and the other side corresponds $\lambda_{1,2} \in \mathbb{C}\backslash\mathbb{R}$. The numerical solution satisfying (15) is presented in Section 3 on the top-right quadrant $(\alpha,\beta) \in \mathbb{R}^2_+$ using the numerical method of polynomials illustrated in [22]. The eigenvalues $\lambda_{1,2}$ are complex conjugate pair if $(\alpha,\beta) \in \mathbb{R}^2_+$ satisfy the inequality

$$\mathcal{T}^2(\alpha,\beta) - 4D(\alpha,\beta) < 0, \tag{16}$$

which leads to an immediate requirement that $D(\alpha,\beta) > 0$. Before proceeding to exploit this requirement note that adding cross-diffusive terms imposes no change to the trace of the stability matrix, implying that the domain-dependent conditions proven in the absence of cross-diffusion presented in [22] will remain valid but only in the form of necessary conditions on the domain-size. In the presence of cross-diffusion, deriving sufficient conditions requires additional work in the sense of exploring the positivity of $D(\alpha,\beta)$. This is because restricting the analysis to exploitation of only the trace of the stability matrix will lead to the same set of conditions obtained with and without cross-diffusion. For the purpose of completeness, we recall the statements of Theorems 1 and 2 in [22].

Theorem 1 (*Condition for Hopf/transcritical Bifurcation*)**.** *Let u and v satisfy the cross-diffusive reaction–diffusion system given by the Eq. (1) with real positive parameters $\alpha > 0$, $\beta > 0$, $d > 0$, and $\gamma > 0$. For the system to exhibit Hopf and/or transcritical bifurcation, the domain-size controlling parameter L must be large enough to satisfy,*

$$L^2 \geq \frac{(d+1)(m^2+n^2)\pi^2}{\gamma}, \tag{17}$$

where m and n are positive integers representing the eigenmodes of the Laplace operator in Ω, with homogeneous Neumann boundary conditions.

Proof. The proof of this theorem depends on the positivity of the trace $\mathcal{T}(\alpha,\beta)$ of the stability matrix given by (9). Note that the trace $\mathcal{T}(\alpha,\beta)$ of the stability of matrix (9) is independent of cross-diffusive coefficients. Thus, the condition of this theorem for the cross-diffusive system remains the same as that in the case of no cross-diffusion, the proof of which is presented in [22]. □

Theorem 2 (*Turing Diffusion-Driven Instability*)**.** *Let u and v satisfy the cross-diffusive reaction–diffusion system given by (1) with real positive parameters $\alpha > 0$, $\beta > 0$, $d > 0$, and $\gamma > 0$. If the domain-size controlling the parameter L satisfies the condition*

$$L^2 < \frac{(d+1)(m^2+n^2)\pi^2}{\gamma} \tag{18}$$

then, the instability of the cross-diffusive system (1) is restricted to Turing type only, which means under this condition temporal periodicity in the dynamics is forbidden. In (18), m and n denote positive integers representing the eigenmodes of the Laplace operator on Ω, with homogeneous Neumann boundary conditions.

Proof. The proof of this theorem is acquired through exploring the real part of the eigenvalues $\lambda_{1,2}$ when the discriminant $\mathcal{T}^2 - 4D$ of the characteristic polynomial is negative. The surface $\mathcal{T}(\alpha,\beta)$ is investigated within the range of the admissible unstable parameter spaces $(\alpha,\beta) \subset \mathbb{R}^2$ using monotonicity and Hessian matrix which leads to condition (18). The interested reader of this proof is referred to Theorem 2 in [22]. Our grounds for exploiting Theorem 2 of [22] in the current analysis is due to the fact that the trace $\mathcal{T}(\alpha,\beta)$ of the stability matrix (9) is independent of d_u and d_v. □

Remark. In the case of self-diffusive systems, Theorem 1 is the necessary condition for the admissibility of temporal periodicity (Hopf/limit cycle behaviour) in the dynamics, however it does not preclude the existence of spatial pattern (Turing type behaviour). Theorem 2, on the other hand, admits the emergence of spatial pattern while totally forbidding the existence of temporal periodicity in the dynamics. Both Theorems 1 and 2 are limited to serve only as necessary conditions for the respected dynamical behaviours in the presence of cross-diffusion. This means, to ensure the expected dynamical behaviours we need further conditions involving relationships between L, d_u, d_v and d. Such conditions are derived by requiring the positivity of the determinant $D(\alpha,\beta)$ of the stability matrix (10).

The determinant of the stability matrix (10) is expanded and factorised in the form of a product of a strictly positive quantity $\frac{1}{\alpha+\beta}$ with a cubic polynomial in β given by [37],

$$D(\alpha,\beta) = p_0 + p_1\beta + p_2\beta^2 + p_3\beta^3, \tag{19}$$

with

$$p_0 = \frac{1}{\alpha+\beta}\kappa_0(\alpha),$$

$$p_1 = \frac{1}{\alpha+\beta}\kappa_1(\alpha),$$
$$p_2 = \frac{1}{\alpha+\beta}\kappa_2(\alpha),$$
$$p_3 = \frac{1}{\alpha+\beta}\kappa_3(\alpha).$$

Here, the κ_i's $(i = 0, 1, 2, 3)$ are expressed in terms of all the remaining parameters of the system written as

$$\kappa_0(\alpha) = \alpha^3\gamma^2 + \alpha^3\gamma k^2 + \alpha d k^4 - \alpha d_u d_v k^4 + \alpha d\gamma k^2 + \alpha^3 d_u\gamma k^2,$$
$$\kappa_1(\alpha) = d k^4 - d_u d_v k^4 - d\gamma k^2 + 3\alpha^2\gamma^2 + 3\alpha^2\gamma k^2 + 3\alpha^2 d_u\gamma k^2 - 2d_v\gamma k^2,$$
$$\kappa_2(\alpha) = 3\alpha\gamma(k^2(d_u+1)+\gamma),$$
$$\kappa_3(\alpha) = \gamma k^2 + \gamma^2 + d_u\gamma k^2 = \gamma(k^2(d_u+1)+\gamma).$$

Note that α and β are non-zero positive constants, hence we can assert that requiring $\mathcal{D}(\alpha,\beta) > 0$ entails the positivity of the cubic polynomial in β given in (19). We start by writing the polynomial such that the coefficient of β^3 is unity, which means we can write

$$\beta^3 + \frac{\kappa_2(\alpha)}{\kappa_3(\alpha)}\beta^2 + \frac{\kappa_1(\alpha)}{\kappa_3(\alpha)}\beta + \frac{\kappa_0(\alpha)}{\kappa_3(\alpha)} > 0. \tag{20}$$

The domain-size controlling constant L is now a parameter of the coefficients of (20). We exploit the following theorem from [49] to deduce the conditions required for (20) to be positive in terms of the parameters of our interest namely L, d, d_u, d_v, γ, and the spectrum of the Laplace operator.

Theorem 3 (*Positivity of a Cubic Polynomial*). *Let $\mathcal{D}(\beta) = \beta^3 + a\beta^2 + b\beta + c$ be a non-degenerate cubic polynomial. For $\mathcal{D}(\beta)$ to be strictly positive, the following conditions must be satisfied:*

(i) $c > 0$,
(ii) $a, b \geq 0$,
(iii) $\Delta(\beta) = a^2b^2 + 18abc - 27c^2 - 4a^3c - 4b^3 \leq 0$,

where $\Delta(\beta)$ represents discriminant of $\mathcal{D}(\beta)$.

Proof. Proof of this theorem is given in [49]. □

Requiring the three conditions on a, b and c in Theorem 3 leads to three inequalities of the form

$$\frac{\kappa_0(\alpha)}{\kappa_3(\alpha)} = \frac{(d - d_u d_v)\alpha k^4 + (\alpha^3\gamma + \alpha d\gamma + \alpha^3 d_u\gamma)k^2 + \alpha^3\gamma^2}{\gamma k^2 + \gamma^2 + d_u\gamma k^2} > 0,$$

$$\frac{\kappa_1(\alpha)}{\kappa_3(\alpha)} = \frac{(d - d_u d_v)k^4 - (d\gamma - 3\alpha^2\gamma - 3\alpha^2 d_u\gamma - 2d_v\gamma)k^2}{\gamma k^2 + \gamma^2 + d_u\gamma k^2} + \frac{3\alpha^2\gamma^2}{\gamma k^2 + \gamma^2 + d_u\gamma k^2} \geq 0, \tag{21}$$

$$\frac{\kappa_2(\alpha)}{\kappa_3(\alpha)} = \frac{3\alpha\gamma^2 + 3\alpha\gamma k^2 + 3\alpha d_u\gamma k^2}{\gamma k^2 + \gamma^2 + d_u\gamma k^2} \geq 0. \tag{22}$$

Proposition 1. *Let the cubic polynomial $\mathcal{D}(\beta)$ in Theorem 3 be defined as*

$$\mathcal{D}(\beta) = h(\beta)\beta + c, \tag{23}$$

where $h(\beta) = \beta^2 + a\beta + b$, for $c > 0$ on $\beta \geq 0$. The nonnegativity of the quadratic polynomial $h(\beta)$ requires

$$a \geq 0,\ b \geq 0,$$

or

$$b > 0,\ 4b \geq a^2.$$

This indicates that the cubic polynomial $\mathcal{D}(\beta)$ is strictly positive for all $\beta \geq 0$ when $c > 0$ [49,50].

The relationship between the domain size controlling parameter L and the cross-diffusive system parameters is stated in the following theorem. The method, we follow in the proof of the next theorem was also followed in the study [37]. However, the condition reached in the study [37] is valid on a disc-shaped geometry, whereas the condition obtained in this study is applied to the rectangular domain and is original in terms of the relationship between domain size and the system parameters.

Theorem 4 (*Condition on L for Spatiotemporal Pattern Formation*). *Let u and v satisfy the cross-diffusive reaction–diffusion system given by the Eq. (1) with real positive parameters $\alpha > 0$, $\beta > 0$, $d > 0$, $\gamma > 0$ and cross-diffusive parameters d_u and d_v. For the cross-diffusive system to exhibit spatiotemporal pattern formation, domain-size controlling parameter L must satisfy the inequality*

$$L^2 > \frac{(d - d_u d_v)(m^2 + n^2)\pi^2}{(7d + 8d_v)\gamma}, \tag{24}$$

where m and n are positive integers representing the eigenmodes of the Laplace operator in Ω, with homogeneous Neumann boundary conditions.

Proof. Direct algebraic manipulation of inequality (22) leads to a trivial requirement of the form $3\alpha \geq 0$, since $(\alpha,\beta) \in \mathbb{R}^2_+$ in System (1). Second condition in Proposition 1 leads to the following condition,

$$3\alpha^2 + \frac{(d - d_u d_v)k^4 - (d + 2d_v)\gamma k^2}{(1 + d_u)\gamma k^2 + \gamma^2} \geq \frac{9\alpha^2}{4}, \tag{25}$$

with

$$\alpha^2 + \frac{(d - d_u d_v)k^4 + d\gamma k^2}{(1 + d_u)\gamma k^2 + \gamma^2} > 0. \tag{26}$$

The conditions (25) and (26) can be simplified as,

$$\frac{4(d - d_u d_v)k^4 - 4(d + 2d_v)\gamma k^2}{(1 + d_u)\gamma k^2 + \gamma^2} \geq -3\alpha^2. \tag{27}$$

and

$$\frac{3(d - d_u d_v)k^4 + 3d\gamma k^2}{(1 + d_u)\gamma k^2 + \gamma^2} > -3\alpha^2. \tag{28}$$

Combination of equal case of (27) and inequality (28) gives the following system,

$$\begin{cases} \dfrac{4(d - d_u d_v)k^4 - 4(d + 2d_v)\gamma k^2}{(1 + d_u)\gamma k^2 + \gamma^2} = -3\alpha^2 \\ \dfrac{3(d - d_u d_v)k^4 + 3d\gamma k^2}{(1 + d_u)\gamma k^2 + \gamma^2} > -3\alpha^2. \end{cases} \tag{29}$$

Substituting for $-3\alpha^2$ from the second part (strict inequality) into the right-hand term of the first equality results in the following inequality

$$\frac{3(d - d_u d_v)k^4 + 3d\gamma k^2}{(1 + d_u)\gamma k^2 + \gamma^2} > \frac{4(d - d_u d_v)k^4 - 4(d + 2d_v)\gamma k^2}{(1 + d_u)\gamma k^2 + \gamma^2}. \tag{30}$$

Solving (30) for k^2 will lead to a sufficient condition on the domain-size controlling parameter L that will ensure the positivity of the cubic polynomial (20) and in turn that of the determinant of the stability matrix given by (19). For the derivation of the desired condition, the sign of the denominator of both sides of (30) is exploited, which requires the analysis to independently investigate the case when the denominator on both sides of (30) is either positive or negative. Such requirement enforces two independent cases to explore, namely $d_u > -1$ and $d_u < -1$, subject to $d - d_u d_v > 0$. Hence, the current analysis admits the concept of cross-diffusion for the activator species to be both negative and positive. However, the determinant of the full matrix must be positive to ensure the regularity of the partial differential system. We exploit the experimental investigation conducted in [4] and results therein, where negative (dimensional values) for cross-diffusion are

demonstrated to give rise to Turing type behaviour in the dynamics. Such experimental findings create the platform to analytically investigate the cross-diffusive parameter d_u across the full spectrum of the real line in particular, both for the choice of negative and positive real values. Therefore, exploiting such observations we first utilise the constraint $d_u > -1$, which entails the positivity of the denominator of both sides of (30). This leads to the inequality

$$3(d - d_u d_v)k^2 + 3d\gamma > 4(d - d_u d_v)k^2 - 4(d + 2d_v)\gamma \tag{31}$$

or

$$3d\gamma + 4(d + 2d_v)\gamma > (d - d_u d_v)k^2. \tag{32}$$

By rearranging the inequality (32), we write,

$$k^2 < \frac{(7d + 8d_v)\gamma}{d - d_u d_v}. \tag{33}$$

Substituting $k^2 = \frac{(m^2 + n^2)\pi^2}{L^2}$ gives the following condition of the domain size L^2 as

$$\frac{(m^2 + n^2)\pi^2}{L^2} < \frac{(7d + 8d_v)\gamma}{d - d_u d_v} \tag{34}$$

or, by rearranging the last expression, we have

$$L^2 > \frac{(d - d_u d_v)(m^2 + n^2)\pi^2}{(7d + 8d_v)\gamma}, \tag{35}$$

which leads to the sufficient condition for the domain size L. □

Remark. The relationship between the main diffusion d and cross-diffusion parameters d_u and d_v is accepted to satisfy $d - d_u d_v > 0$ for the system to be well-posed. The proof of this relationship has been presented in [7]. Therefore, the current analysis is based on the fact that $d - d_u d_v > 0$.

3. Numerical generation of the parameter spaces

In this section, numerical simulations of the parameter spaces satisfying the conditions derived from the previous section are presented on the plane $(\alpha, \beta) \in \mathbb{R}^2_+$. For illustrative purposes, all computations are carried out on a unit square domain, unless stated otherwise. We will explore the generation of parameter spaces when the domain length and the modes m and n are varied (see Table 2 for details and finite element simulations shown in Fig. 17). In addition, we demonstrate the calculation of the implicit partition curves. The partitioning curves that separate the real and imaginary parts must satisfy,

$$\mathcal{T}^2 - 4D = 0, \tag{36}$$

which corresponds to the repeated roots of the eigenvalues. The change of the sign of the discriminant $\mathcal{T}^2 - 4D$ establishes the real and complex regions, respectively. Moreover, solution of Eq. (36) determines the boundary of these regions. On the other hand, solutions of Eq. (36) can be represented implicitly by the following polynomial of order six in β, where the coefficients depend on the other system parameters in the form

$$\begin{aligned}\psi(\alpha, \beta) &= P_0(\alpha_i) + P_1(\alpha_i)\beta + P_2(\alpha_i)\beta^2 + P_3(\alpha_i)\beta^3 \\ &\quad + P_4(\alpha_i)\beta^4 + P_5(\alpha_i)\beta^5 + P_6(\alpha_i)\beta^6,\end{aligned} \tag{37}$$

where

$$\begin{aligned}P_0 &= \gamma^2\alpha^6 + 2\gamma\alpha^4(-\gamma + (d - 2d_u - 1)k^2) \\ &\quad + \gamma^2\alpha^2 - 2k^2\alpha^2(d - 1)\gamma + \alpha^2(d + 4d_u d_v - 2d + 1)k^4,\end{aligned}$$

$$\begin{aligned}P_1 &= 6\gamma^2\alpha^5 - 12\gamma^2\alpha^3 + 8\gamma\alpha^3(d - 2d_u - 1)k^2 \\ &\quad - \gamma^2 - 4d_v k^2 + (d^2 + 4d_u d_v - 2d + 1)k^4\end{aligned}$$

$$P_2 = 15\gamma^2\alpha^4 - 24\gamma\alpha^2 + 12\gamma\alpha^2(d - 2d_u - 1)k^2$$

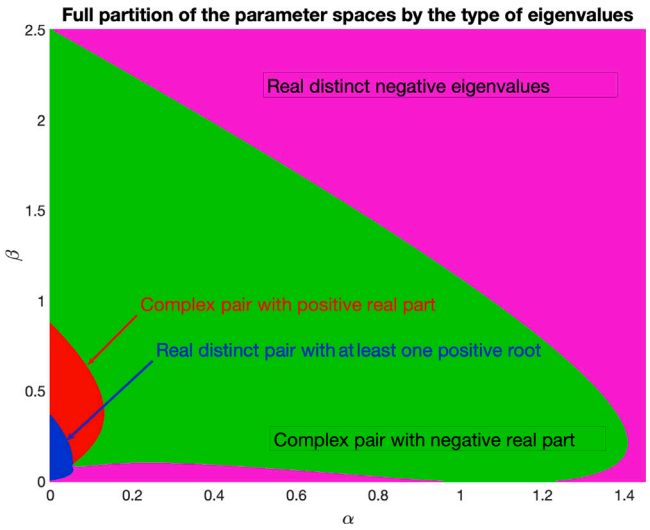

Fig. 1. Classification of the parameter spaces for the stability regions of the reaction–diffusion system in the presence of linear cross-diffusion with $d = 1$, $d_u = d_v = 0.1$, and $\gamma = 100$ (For interpretation of the references to colour in this figure legend, the readeris referred to the web version of this article).

$$+\gamma^2 + 2k^2(d + 4d_v - 1) + \gamma + (d^2 + 4d_u d_v - 2d + 1)k^4,$$

$$P_3 = 5\alpha^3\gamma - 5\gamma^2\alpha + 8\gamma\alpha(d - 2d_u - 1)k^2$$

$$P_4 = 15\gamma^2\alpha^2 - 6\gamma^2 + 2\gamma(d - 2d_u - 1)k^2$$

$$P_5 = 6\alpha\gamma^2,$$

$$P_6 = \gamma^2.$$

The classification of parameter spaces on the (α, β) plane is presented in Fig. 1 where the cross-diffusion parameters are now included. In the regions in which the real part of the eigenvalues (whether purely real or complex) is positive represent unstable regions whereby the uniform steady state solution (u_s, v_s) is asymptotically unstable, while those regions where the real part of the eigenvalues is negative represent stable regions for the uniform steady state solution. Regions that allow for Turing pattern formation to occur are those associated with the instability of the uniform steady state solution for the case of real eigenvalues, while the case of complex eigenvalues will give rise to oscillatory solutions. In Fig. 1, the curve that divides regions given by green and magenta colours shows the boundary for real and complex eigenvalues, in which the discriminant is $\mathcal{T}^2 - 4D = 0$. Regions containing the complex eigenvalues are indicated with green and red colours, and regions containing real eigenvalues are indicated by magenta and blue colours. In addition, the boundary curve which divides magenta and green regions, corresponds to the real repeated negative eigenvalues. Model parameters chosen from these regions will result in the reaction–diffusion system with linear cross-diffusion converging to the uniform steady state. Here, the magenta colour region corresponds to the real distinct negative eigenvalues, in which the choice of (α, β) within this region entails that the uniform steady state solution (u_s, v_s) becomes stable. The green region is also a stable region with complex eigenvalues possessing negative real part. Again the choice of the parameters from this region will ensure that the uniform steady state solution is asymptotically stable. The curve that divides the green and red regions represents the separation of the stable and unstable parameter spaces. The red and blue regions (or spaces) are where the uniform steady state solution is asymptotically unstable. Parameters from this blue region have the potential to give rise to Turing patterns under appropriate cross-diffusive driven instability conditions. The red

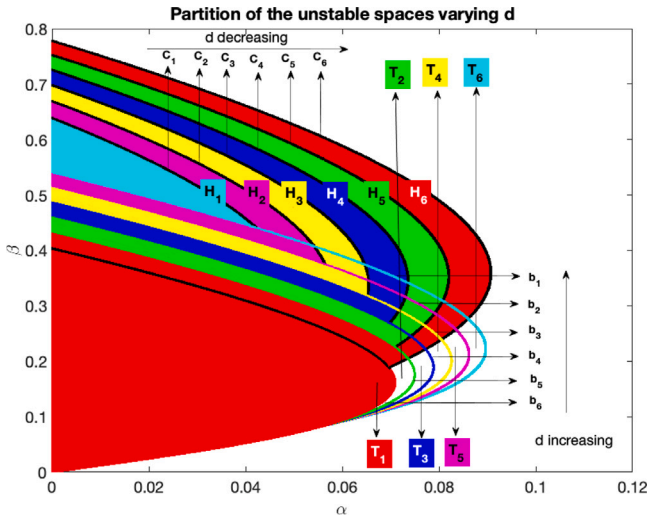

Fig. 2. Parameter spaces of the reaction–diffusion system in the presence of linear cross-diffusion for different diffusion coefficients d and fixed $d_u = 0.1$, $d_v = 0.1$ and $\gamma = 100$.

region is obtained when the eigenvalues are complex with a positive real part, in which we have the Hopf bifurcation region. Furthermore, the curve that separates the red and blue regions corresponds to the eigenvalues that are real and repeated and the blue region is the region where the eigenvalues are real and at least one of them is positive. The domain size satisfying the condition given by Theorem 4 is provided in the numerical simulations section for the selected parameter values.

Investigation of the spatial patterns, temporally periodic patterns and limit cycle behaviour of the system are conducted through variations of the main diffusion coefficient d and cross-diffusion parameters d_u and d_v, all satisfying the conditions of theorems presented in Section 2. In each of the figures illustrating the parameter spaces with variation of each of the three parameters (d, d_u, d_v), the curves b_1 to b_6 represent Turing space boundaries. In Fig. 2, parameter spaces are presented for varying d when the cross-diffusion parameters d_u and d_v are fixed. Results showing the Hopf bifurcation regions are represented by H_1-H_6, whereas the transcritical curves are shown by c_1-c_6. Observations from Fig. 2 indicate that decreasing d results in an increase of the Hopf bifurcation region. We also observe that the limit cycle curves shift from c_1 to c_6 as d decreases. On the other hand, an increase in d results in an increase in Turing regions, unlike Hopf and transcritical type of bifurcation regions.

Fig. 3(a) presents the regions for variations of d_u when d and d_v are fixed. Assuming the cross-diffusion coefficient $d_u > 0$, increasing d_u does not change the limit cycle behaviour. On the other hand, an increase in d_u results in the shrinking of the Hopf bifurcation regions downwards from H_1 to H_6. From Fig. 3(a), we observe that Turing regions start to invade the Hopf bifurcation regions gradually as d_u increases.

Fig. 3(b) indicates the regions for variations of d_v when d and d_u values are fixed. Variation of d_v gives the same location of limit cycle curve as in Fig. 3(a). Increase of parameters d_u and d_v results in as expansion of Turing regions. This can be observed by Turing space boundaries as d_v values gets varied. Hence, we can conclude from Fig. 3 that variations of positive cross-diffusion coefficients d_u and d_v do not affect the limit cycle behaviour, only the Turing parameter space regions do change with variations in the cross-diffusion coefficients.

Next, we generate parameter spaces by considering negative cross-diffusion coefficients d_u and d_v. These spaces exists for the reaction–diffusion system only in the presence of linear cross-diffusion. By taking the principal diffusion coefficient $d = 1$, we ensure that the reaction–diffusion system in the absence of cross-diffusion does not give rise to regions of instability. Fig. 4(a) shows the effect of negative cross-diffusion on the regions corresponding to the Hopf/transcritical curves for $d_u \in (-1, 0)$ satisfying the condition given by Theorem 4. As in Fig. 3(a), the limit cycle curve does not change the position with variations in d_u. However, the Hopf/transcritical bifurcation regions decrease as d_u gets closer to -1. In Fig. 4(b), the effect of negative cross-diffusion on Turing spaces is presented for $d_u \in (-1, 0)$.

Remark. The parameter spaces provided in Figs. 1, 2, 3 and 4 and their summary presented in Table 1 are generated using $L = 1$ and varying the self- and cross-diffusion coefficients d, d_u and d_v, while keeping all the remaining parameters and eigenmodes $m = 1$ and $n = 1$ fixed.

While the inequalities m and n suggest a theoretical range that extends to infinity, this does not imply that $L^2 = \infty$ is physically meaningful or applicable within the context of the model defined in System (1). The conditions we derived in Theorems 1, 2, and 4 are valid and practical within the bounds of a finite domain where the foundational assumptions for pattern formation and diffusion-driven instability hold true. Once these assumptions are violated in the limits of an infinite domain, the model itself becomes invalid for predicting or generating Turing (spatial) or Hopf (spatiotemporal) patterns. Given that these essential criteria are met, we have conducted simulations across various parameter spaces to demonstrate both Turing-type and Hopf bifurcations, which result in spatial and spatiotemporal pattern formation in System (1). Table 2 specifically illustrates simulations for larger eigenmodes, thereby validating the claims made in Theorems 1, 2, and 4. These figures in Table 2 clearly show that, under the appropriate conditions, System (1) indeed undergoes the predicted instabilities and pattern formation as stated in our theorems. Table 1 in conjunction with Figs. 2 and 3 are novel results which succinctly summarises the full classification of the admissible parameter space, and predicts the expected dynamical properties of the RDS, provided that parameters are selected from the given regions. These are in turn simulated for all types of instabilities using the finite element method.

4. Finite element numerical simulations of the reaction-diffusion system with linear cross-diffusion

In this section, we present numerical simulations of the model System (1) to validate the theoretical findings by using the finite element method. For details on the finite element method, theory and applications, the interested reader is referred to the seminal work in [51], and references therein. Simulations are all performed on a rectangular domain using a uniform triangular mesh. Initial conditions are chosen by considering small random perturbations around the uniform steady-state, for example, in the form of [21,22],

$$u_0(x, y) = \alpha + \beta + 0.0016\cos(2\pi(x + y)) + 0.01\sum_{i=0}^{8}\cos(i\pi x), \quad \text{and}$$

$$v_0(x, y) = \frac{\beta}{(\alpha + \beta)^2} + 0.0016\cos(2\pi(x + y)) + 0.01\sum_{i=0}^{8}\cos(i\pi x).$$

In our numerical simulations, we select model parameters α and β from the parameter spaces presented in Section 3. The parameter values used in the numerical simulations are summarised in Table 1. In all our finite element simulations, we take 8192 triangular elements, yielding 8450 degrees of freedom. To march forward in time, we use the 1st order semi-implicit backward differential formula (1-SBEM) as presented and validated in [52] with timestep $\Delta t = 0.0025$. These parameters for the finite element algorithm ensure stability and convergence of the numerical method.

In our first example, we select model parameters outside the parameter spaces as $d = 2$, $\gamma = 100$, $d_u = d_v = 0.1$, $\alpha = 0.5$ and $\beta = 1.5$, such that no spatiotemporal patterns can emerge. The only stable solution is the homogeneous uniform steady state. Fig. 5(a)

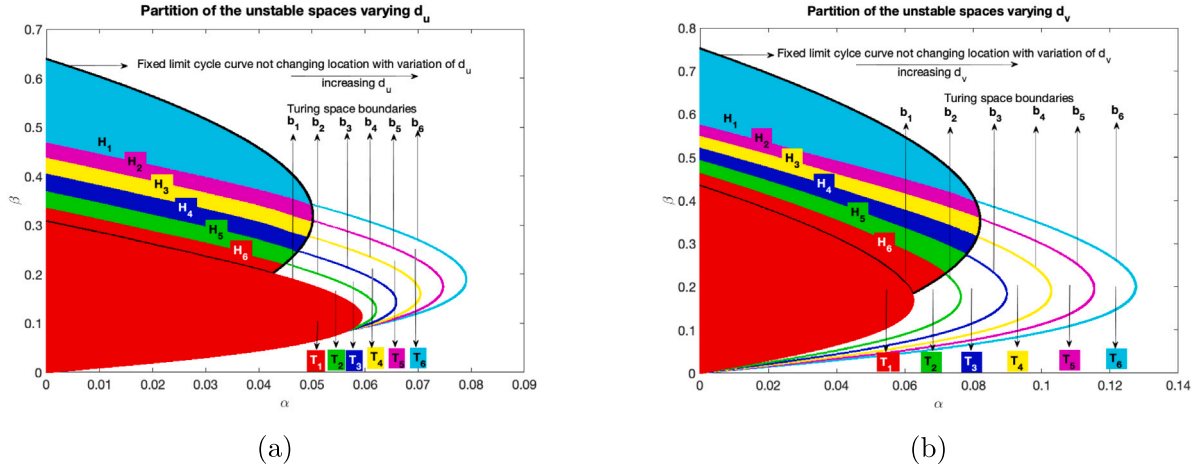

Fig. 3. (a) Parameter spaces generated by the reaction–diffusion system with linear cross-diffusion when $d_u > 0$ is varied positively for fixed $d = 2$ and $d_v = 0.1$ and $\gamma = 100$ (b) Parameter spaces generated by the reaction–diffusion system with linear cross-diffusion when $d_v > 0$ is varied positively for fixed $d = 1.2$, $d_u = 0.1$ and $\gamma = 100$.

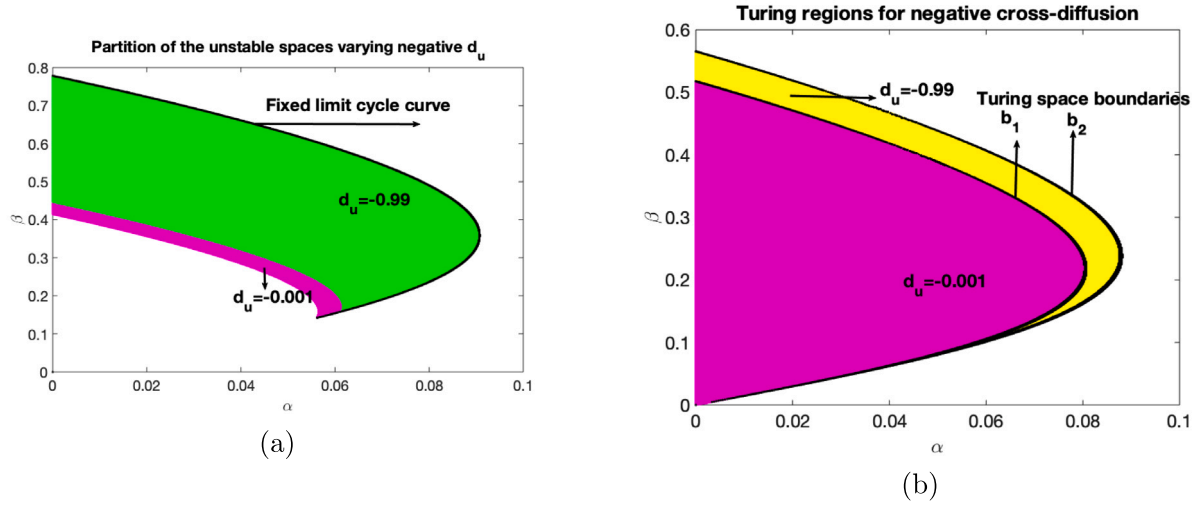

Fig. 4. (a) Parameter spaces for the reaction–diffusion system with linear cross-diffusion exhibiting regions with hopf/transcritical bifurcations for negative cross-diffusion coefficient d_u while the rest of the parameters are fixed as $d = 1$, $d_v = 0.01$ and $\gamma = 100$ (b) Turing spaces generated for the reaction–diffusion system with linear cross-diffusion coefficient d_u varied and for fixed $d = 1.2$, $d_v = 0.01$ and $\gamma = 100$.

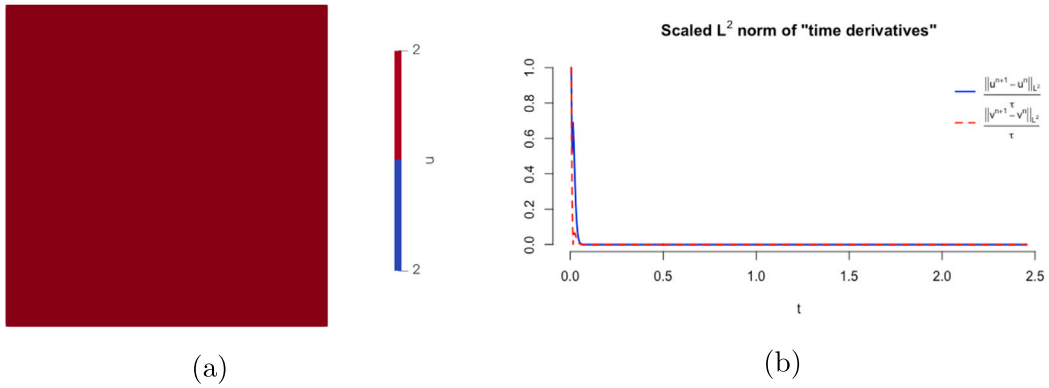

Fig. 5. (a) Finite element numerical solution corresponding to the $u-$ component of the reaction–diffusion system (1) with linear cross-diffusion. A uniform steady state solution is observed in complete agreement with theoretical predictions, with $d = 2$, $\gamma = 100$, $d_u = d_v = 0.1$, $\alpha = 0.5$ and $\beta = 1.5$. (b) The plot of the L_2 norm of the discrete time-derivative of the finite element solutions u and v.

Table 1
Full classification of parameter spaces for all types of bifurcations (USS: Uniform Steady-State).

Dynamics near USS (u_s, v_s)			Convergence to USS (No pattern formation)	Spatial pattern formation		Spatiotemporal pattern formation	
Types of USS (u_s, v_s)			Stable node/spiral	Turing space boundaries (Unstable star node)	Turing spaces (Unstable node)	Hopf bifurcation spaces (Unstable spiral)	Limit cycle curves (Transcritical bifurcation)
		(d, d_u, d_v, γ)	$\lambda_{1,2}$				
			$0 > \lambda_{1,2} \in \mathbb{R}$ or $\lambda_{1,2} \in \mathbb{C}\backslash\mathbb{R}, \mathrm{Re}(\lambda) < 0$	$\lambda_{1,2} \in \mathbb{R}, 0 < \lambda_1 = \lambda_2$	$0 < \lambda_1 \in \mathbb{R}$ or $0 < \lambda_2 \in \mathbb{R}$	$\lambda_{1,2} \in \mathbb{C}\backslash\mathbb{R},\ \mathrm{Re}(\lambda_{1,2}) > 0$	$\lambda_{1,2} \in \mathbb{C}\backslash\mathbb{R},\ \mathrm{Re}(\lambda_{1,2}) = 0$
Varying d	Fig. 2	(1.0, 0.1, 0.1, 100)	$\mathbb{R}^2_+ \backslash T_1 \cup \bigcup_{i=1}^{6} H_i$	Curve b_6	T_1	$\bigcup_{i=1}^{6} H_i$	Curve c_6
		(1.2, 0.1, 0.1, 100)	$\mathbb{R}^2_+ \backslash \bigcup_{i=1}^{2} T_i \cup \bigcup_{i=1}^{5} H_i$	Curve b_5	$\bigcup_{i=1}^{2} T_i$	$\bigcup_{i=1}^{5} H_i$	Curve c_5
		(1.4, 0.1, 0.1, 100)	$\mathbb{R}^2_+ \backslash \bigcup_{i=1}^{3} T_i \cup \bigcup_{i=1}^{4} H_i$	Curve b_4	$\bigcup_{i=1}^{3} T_i$	$\bigcup_{i=1}^{4} H_i$	Curve c_4
		(1.6, 0.1, 0.1, 100)	$\mathbb{R}^2_+ \backslash \bigcup_{i=1}^{4} T_i \cup \bigcup_{i=1}^{3} H_i$	Curve b_3	$\bigcup_{i=1}^{4} T_i$	$\bigcup_{i=1}^{3} H_i$	Curve c_3
		(1.8, 0.1, 0.1, 100)	$\mathbb{R}^2_+ \backslash \bigcup_{i=1}^{5} T_i \cup \bigcup_{i=1}^{2} H_i$	Curve b_2	$\bigcup_{i=1}^{5} T_i$	$\bigcup_{i=1}^{2} H_i$	Curve c_2
		(2.0, 0.1, 0.1, 100)	$\mathbb{R}^2_+ \backslash \bigcup_{i=1}^{6} T_i \cup H_1$	Curve b_1	$\bigcup_{i=1}^{6} T_i$	H_1	Curve c_1
		(d, d_u, d_v, γ)	$\lambda_{1,2}$				
			$0 > \lambda_{1,2} \in \mathbb{R}$ or $\lambda_{1,2} \in \mathbb{C}\backslash\mathbb{R}, \mathrm{Re}(\lambda) < 0$	$\lambda_{1,2} \in \mathbb{R}, 0 < \lambda_1 = \lambda_2$	$0 < \lambda_1 \in \mathbb{R}$ or $0 < \lambda_2 \in \mathbb{R}$	$\lambda_{1,2} \in \mathbb{C}\backslash\mathbb{R},\ \mathrm{Re}(\lambda_{1,2}) > 0$	$\lambda_{1,2} \in \mathbb{C}\backslash\mathbb{R},\ \mathrm{Re}(\lambda_{1,2}) = 0$
Varying d_u	Fig. 3(a)	(2, 2, 0.1, 100)	$\mathbb{R}^2_+ \backslash T_1 \cup \bigcup_{i=1}^{6} H_i$	Curve b_1	T_1	$\bigcup_{i=1}^{6} H_i$	Fixed
		(2, 4, 0.1, 100)	$\mathbb{R}^2_+ \backslash \bigcup_{i=1}^{2} T_i \cup \bigcup_{i=1}^{5} H_i$	Curve b_2	$\bigcup_{i=1}^{2} T_i$	$\bigcup_{i=1}^{5} H_i$	Fixed
		(2, 6, 0.1, 100)	$\mathbb{R}^2_+ \backslash \bigcup_{i=1}^{3} T_i \cup \bigcup_{i=1}^{4} H_i$	Curve b_3	$\bigcup_{i=1}^{3} T_i$	$\bigcup_{i=1}^{4} H_i$	Fixed
		(2, 9, 0.1, 100)	$\mathbb{R}^2_+ \backslash \bigcup_{i=1}^{4} T_i \cup \bigcup_{i=1}^{3} H_i$	Curve b_4	$\bigcup_{i=1}^{4} T_i$	$\bigcup_{i=1}^{3} H_i$	Fixed
		(2, 13, 0.1, 100)	$\mathbb{R}^2_+ \backslash \bigcup_{i=1}^{5} T_i \cup \bigcup_{i=1}^{2} H_i$	Curve b_5	$\bigcup_{i=1}^{5} T_i$	$\bigcup_{i=1}^{2} H_i$	Fixed
		(2, 18, 0.1, 100)	$\mathbb{R}^2_+ \backslash \bigcup_{i=1}^{6} T_i \cup H_1$	Curve b_6	$\bigcup_{i=1}^{6} T_i$	H_1	Fixed
		(d, d_u, d_v, γ)	$\lambda_{1,2}$				
			$0 > \lambda_{1,2} \in \mathbb{R}$ or $\lambda_{1,2} \in \mathbb{C}\backslash\mathbb{R}, \mathrm{Re}(\lambda) < 0$	$\lambda_{1,2} \in \mathbb{R}, 0 < \lambda_1 = \lambda_2$	$0 < \lambda_1 \in \mathbb{R}$ or $0 < \lambda_2 \in \mathbb{R}$	$\lambda_{1,2} \in \mathbb{C}\backslash\mathbb{R},\ \mathrm{Re}(\lambda_{1,2}) > 0$	$\lambda_{1,2} \in \mathbb{C}\backslash\mathbb{R},\ \mathrm{Re}(\lambda_{1,2}) = 0$
Varying d_v	Fig. 3(b)	(1.2, 0.1, 0.01, 100)	$\mathbb{R}^2_+ \backslash T_1 \cup \bigcup_{i=1}^{6} H_i$	Curve b_1	T_1	$\bigcup_{i=1}^{6} H_i$	Fixed
		(1.2, 0.1, 0.11, 100)	$\mathbb{R}^2_+ \backslash \bigcup_{i=1}^{2} T_i \cup \bigcup_{i=1}^{5} H_i$	Curve b_2	$\bigcup_{i=1}^{2} T_i$	$\bigcup_{i=1}^{5} H_i$	Fixed
		(1.2, 0.1, 0.21, 100)	$\mathbb{R}^2_+ \backslash \bigcup_{i=1}^{3} T_i \cup \bigcup_{i=1}^{4} H_i$	Curve b_3	$\bigcup_{i=1}^{3} T_i$	$\bigcup_{i=1}^{4} H_i$	Fixed
		(1.2, 0.1, 0.31, 100)	$\mathbb{R}^2_+ \backslash \bigcup_{i=1}^{4} T_i \cup \bigcup_{i=1}^{3} H_i$	Curve b_4	$\bigcup_{i=1}^{4} T_i$	$\bigcup_{i=1}^{3} H_i$	Fixed
		(1.2, 0.1, 0.41, 100)	$\mathbb{R}^2_+ \backslash \bigcup_{i=1}^{5} T_i \cup \bigcup_{i=1}^{2} H_i$	Curve b_5	$\bigcup_{i=1}^{5} T_i$	$\bigcup_{i=1}^{2} H_i$	Fixed
		(1.2, 0.1, 0.51, 100)	$\mathbb{R}^2_+ \backslash \bigcup_{i=1}^{6} T_i \cup H_1$	Curve b_6	$\bigcup_{i=1}^{6} T_i$	H_1	Fixed

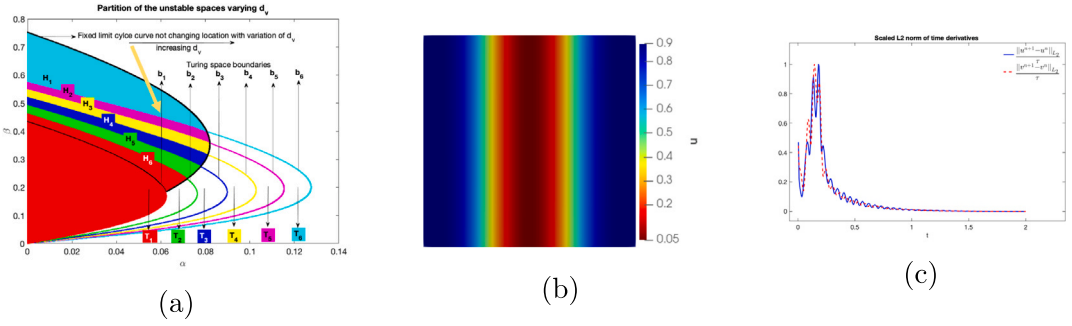

Fig. 6. (a) Parameter space on which we choose $\alpha = 0.06$ and $\beta = 0.48$ with the rest of the model parameters chosen fixed as $d = 1.2$, $\gamma = 100$, $d_u = 0.1$, and $d_v = 0.51$ such that the Turing diffusion-driven instability conditions are satisfied. (b) Finite element solution corresponding to the $u(t, \mathbf{x})$ variable illustrating the formation of a spatially time-independent inhomogeneous stripe pattern. (c) A plot of the L_2-norm of the discrete time-derivative of the solutions u and v.

presents the effect of these parameter choices from the region where the uniform steady state is the only stable solution, thereby giving rise to no spatiotemporal patterns as expected. Fig. 5(b), presents the uniform convergence to the steady state (u_s, v_s) showing the L_2-norm of the discrete time derivatives of the solutions u and v. The evolution of the L_2 norm demonstrates the temporal evolution of the convergence of the finite element method when solving the reaction–diffusion system with linear cross-diffusion to the uniform steady state, with no growth in the norm.

Next, we select model parameters from the Turing diffusion-driven instability parameter space shown in Fig. 6(a). Fig. 6(b) illustrates the formation of a time-independent spatially inhomogeneous solution of the reaction–diffusion system for the selected model parameters. The model parameters are chosen such that these satisfy the conditions

Table 2
Generation of the cross-diffusion -driven parameter spaces varying L and the modes m and n.

$L = 1$ with $(d, d_u, d_v, \gamma) = (1, 0.1, 0.55, 155)$			
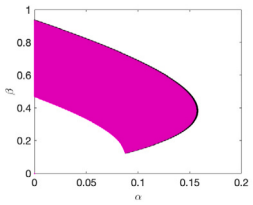 $m = 1, n = 0$	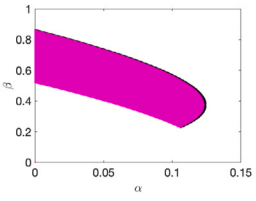 $m = 1, n = 1$	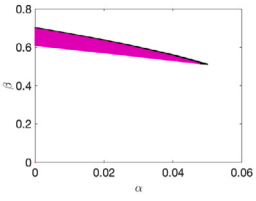 $m = 2, n = 0$	For $m \geq 2$, $n \geq 1$ continuous decrease of parameter spaces lead to extinction of Hopf and transcritical bifurcation
$L = 2$ with $(d, d_u, d_v, \gamma) = (1, 0.1, 0.55, 155)$			
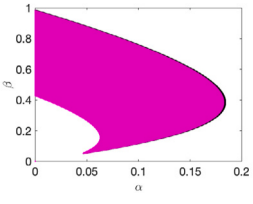 $m = 1, n = 0$	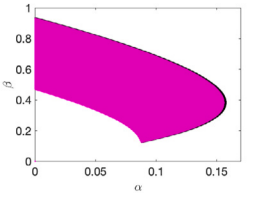 $m = 2, n = 0$	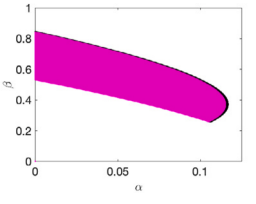 $m = 3, n = 0$	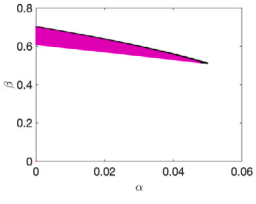 $m = 4, n = 0$
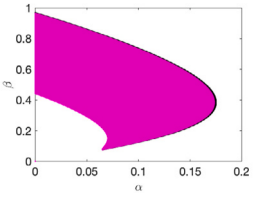 $m = 1, n = 1$	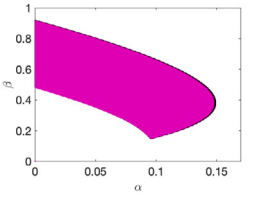 $m = 2, n = 1$	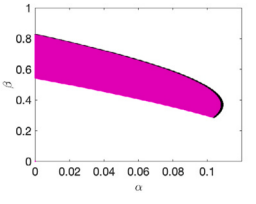 $m = 3, n = 1$	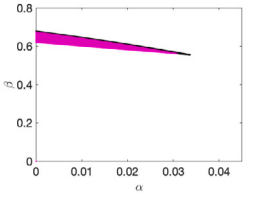 $m = 4, n = 1$
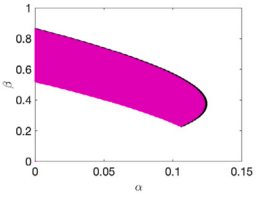 $m = 2, n = 2$	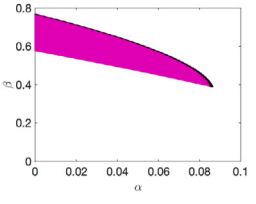 $m = 3, n = 2$	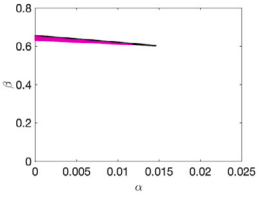 $m = 3, n = 3$	For $m \geq 4$, $n \geq 2$ continuous decrease of parameter spaces lead to extinction of Hopf and transcritical bifurcation

given in Theorems 1 and 4. To demonstrate the temporal evolution of the pattern forming process, we plot the discrete L_2 norm of the discrete time derivative of both finite element solutions as illustrated in Fig. 6(c). At the early stages of the finite element simulation, diffusion dominates, leading to a rapid and sharp decrease in the L_2 norm. This is followed by an exponential-like increase in the L_2 due to the growing excitable modes, leading to the formation of the spatial pattern. The growth is finally bounded, whereby the nonlinear terms start to become dominant, leading to a smooth decrease in the L_2 norm. It is during this last phase that the solutions converge to a time-independent spatially inhomogeneous pattern [1,2].

To illustrate the validity of Theorems 1 and 4 (conditions (17) and (24)), in Figs. 7–8–9, we exhibit periodic pattern formation when model parameters are selected from the Hopf/transcritical bifurcation parameter spaces. The spatiotemporal dynamics of the reaction–diffusion system with linear cross-diffusion exhibit temporal periodicity in their L_2 norms that are of equal amplitudes. These clearly demonstrate the limit cycle behaviour of the system. To further support this claim, we have plotted snap shots of the spatial patterns at discrete time intervals, picked appropriately to illustrate the formation of spatial structure that is continuously evolving in time. For example, in Fig. 7, at time approximately 0.175, at the time of the peak of the L_2 norm, a spot pattern is observed. However, this pattern only exists for a short fixed finite time, before it looses its stability, with the system converging to a spatially homogeneous steady state, when the L_2 norm decays to zero (see the uniform spatial pattern at time approximately 0.4). The spot pattern remerges again (or could be a different one as

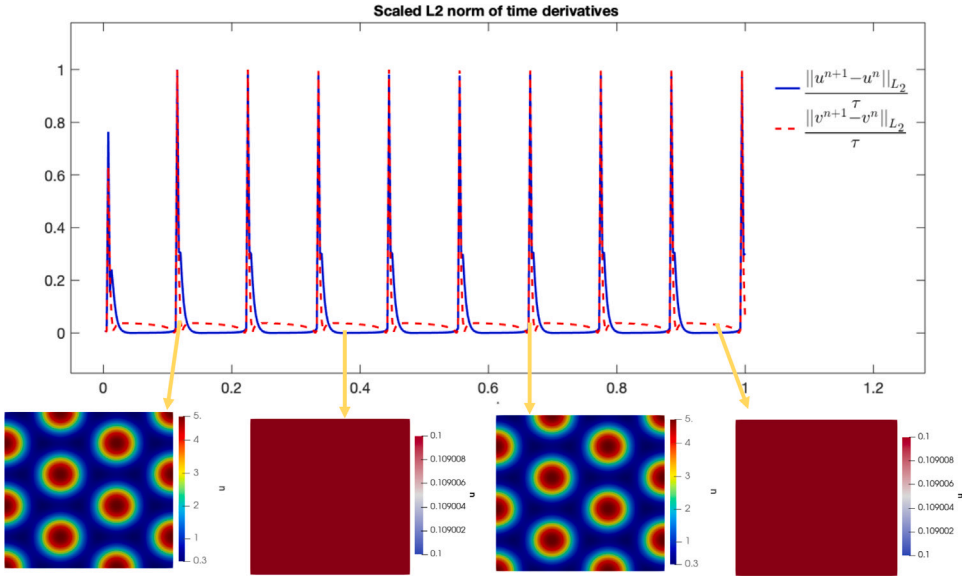

Fig. 7. Finite element simulations corresponding to the u-component of the reaction–diffusion system (1) with linear cross-diffusion. Parameter values are selected to satisfy conditions (17) and (24) of Theorems 1 and 4, respectively, with $d = 12$, $\gamma = 320$, $d_u = 0.001$, $d_v = 2.8$, $\alpha = 0.075$ and $\beta = 0.15$.

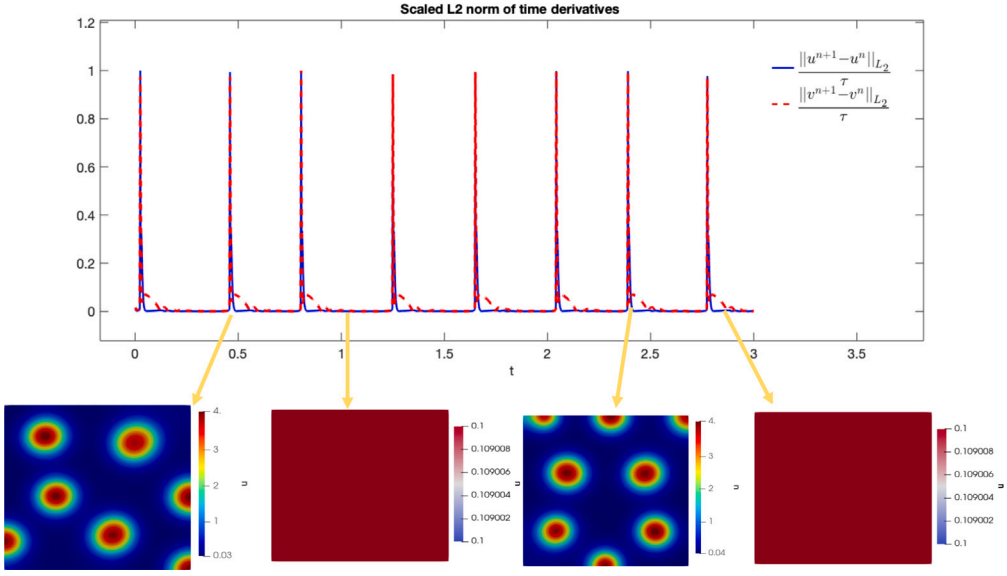

Fig. 8. Finite element simulations corresponding to the u-component of the reaction–diffusion system (1) with linear cross-diffusion. Parameter values are selected to satisfy conditions (17) and (24) of Theorems 1 and 4, respectively, with $d = 12$, $\gamma = 410$, $d_u = 0.001$, $d_v = 2.8$, $\alpha = 0.1$ and $\beta = 0.1$.

shown next) when the L_2 norm is increasing, as illustrated at say, time approximately 0.645. This cyclic behaviour in the model system confirms the theoretical predictions stated in Theorems 1 and 4.

In Figs. 8–9 we exhibit similar cyclic behaviour; the plots of the discrete L_2 norm of the discrete time-derivative show periodicity in pattern formation. Unlike the case of Fig. 7, different spot patterns are converged to at different amplitudes of the L_2 norm. We conjecture that the reaction–diffusion system with linear cross-diffusion gains and looses stability at different branches within the limit cycle behaviour, with some solutions repeated periodically, while at times, these are not repeated periodically (these could be out of phase for example).

In all the examples given by Figs. 7–9, once the spatially heterogeneous solution becomes unstable, the reaction–diffusion system with linear cross-diffusion tends to converge to a spatially uniform steady state. This uniform steady state is not unique, it depends on how close the spatially heterogeneous solution is to the uniform steady state. Further studies on the bifurcation pathways of the system given the spatial pattern formation are required in order to fully understand the transition modes during this cyclic behaviour.

Fig. 10 shows the simulation for the choice of parameter values satisfying the conditions of Theorems 1 and 4, giving rise to the spatiotemporal periodicity. The choice of the main diffusion coefficient $d = 1$ admits that the eigenvalues to be complex with positive real

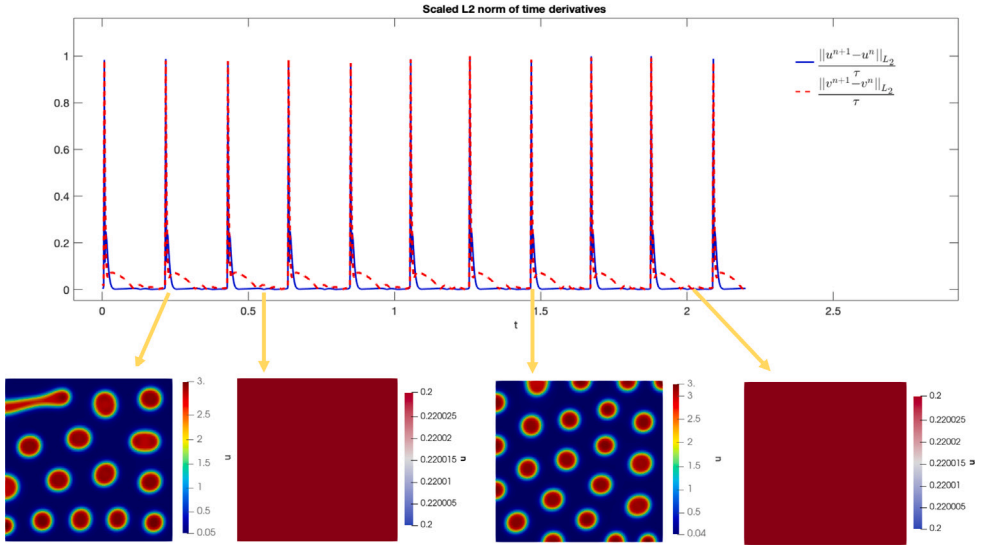

Fig. 9. Finite element simulations corresponding to the u-component of the reaction–diffusion system (1) with linear cross-diffusion. Parameter values are selected to satisfy conditions (17) and (24) of Theorems 1 and 4, respectively, with $d = 12.15$, $\gamma = 390$, $d_u = 4$, $d_v = 2.8$, $\alpha = 0.1$ and $\beta = 0.1$.

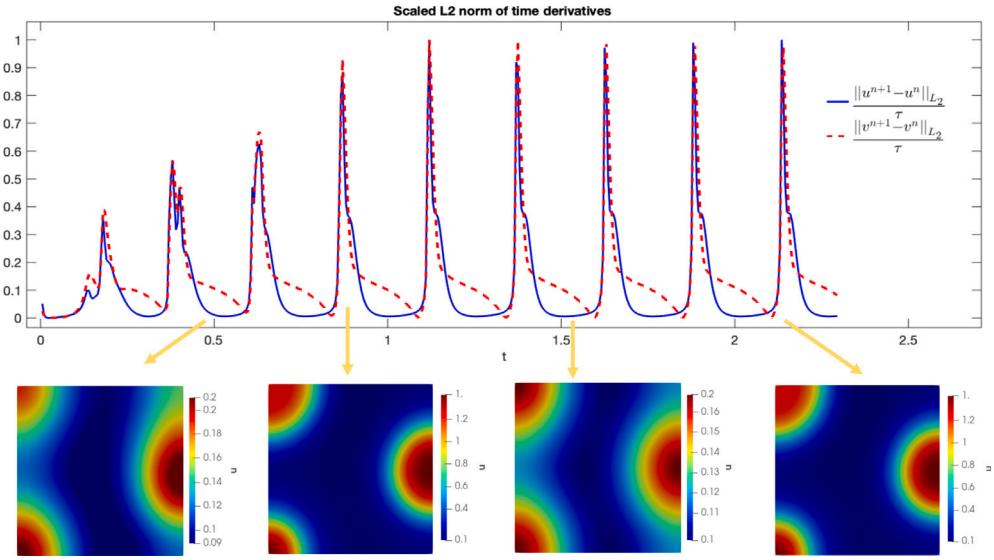

Fig. 10. Finite element simulations corresponding to the u-component of the reaction–diffusion system (1) with linear cross-diffusion. Parameter values are selected to satisfy conditions (17) and (24) of Theorems 1 and 4, respectively, with $d = 1$, $\gamma = 155$, $d_u = 0.01$, $d_v = 0.55$, $\alpha = 0.085$ and $\beta = 0.1$.

part. One important observation of the selection of the parameter $d = 1$ is that it is now possible to have patterns in the dynamics only in the presence of cross-diffusion. The plot of L_2 for the discrete time-derivative shows the temporal patterning with equal amplitudes. Unlike the previous cases shown in Figs. 7–9, we observe the transition of spatially inhomogeneous solutions for each stage. Limit cycles are observed for long term dynamical behaviour of the system.

Fig. 11 exhibits the Hopf type of bifurcation for the choice of parameter spaces satisfying the conditions of Theorems 1 and 4. In this particular example, we select the main diffusion coefficient as $d = 1$ in the presence of the negative cross-diffusion. One other difference of this experiment from the example shown in Fig. 10 is the usage of larger γ values, giving rise to larger positive values in the trace of the stability matrix meaning that the positive real part of the complex eigenvalues is larger. The plot of L_2 norm of the discrete time derivative shows the spatiotemporal patterning with a decaying amplitude. In the long term dynamics, we observe temporal cycles are getting smaller. The decay in amplitude reflects the fact that the reaction–diffusion system with linear cross-diffusion is converging to spatially inhomogeneous solutions in a time-periodic fashion.

4.1. Exploration of the parameter spaces and their impact on pattern formation

In this section, we aim to investigate the effect of parameter choice on the analysis of the pattern formation in light of the theoretical observations related to the domain size and the cross-diffusive system. We present the full model parameters and their choices and the type of pattern the model system exhibits, in the captions of each Figure.

We begin with the case when the domain size L^2 satisfies Theorems 2 and 4 (i.e. the domain size fulfils conditions (18) and (24)). In this numerical experiment we observe that the type of instability for

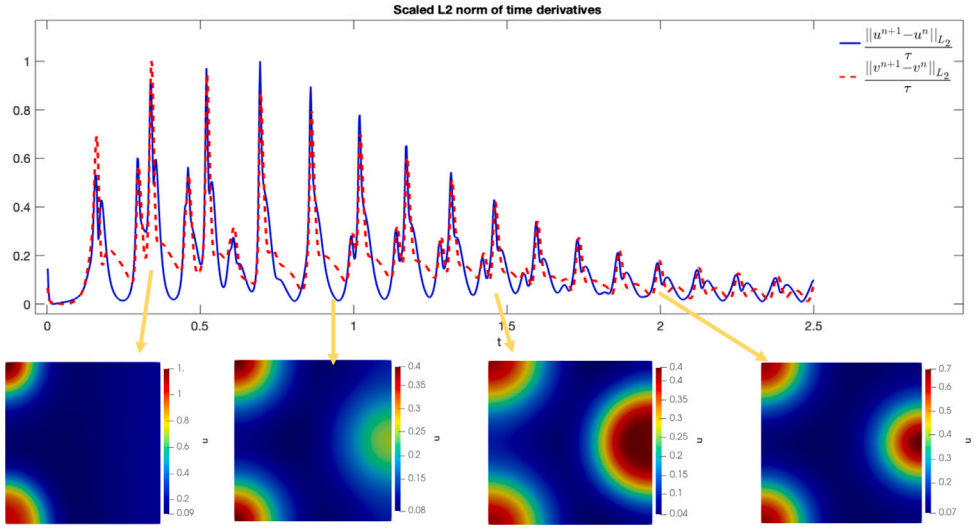

Fig. 11. Finite element simulations corresponding to the u-component of the reaction–diffusion system (1) with linear cross-diffusion. Parameter values are selected to satisfy conditions (17) and (24) of Theorems 1 and 4, respectively, with $d = 1$, $\gamma = 192$, $d_u = -0.01$, $d_v = 0.5$, $\alpha = 0.085$ and $\beta = 0.1$.

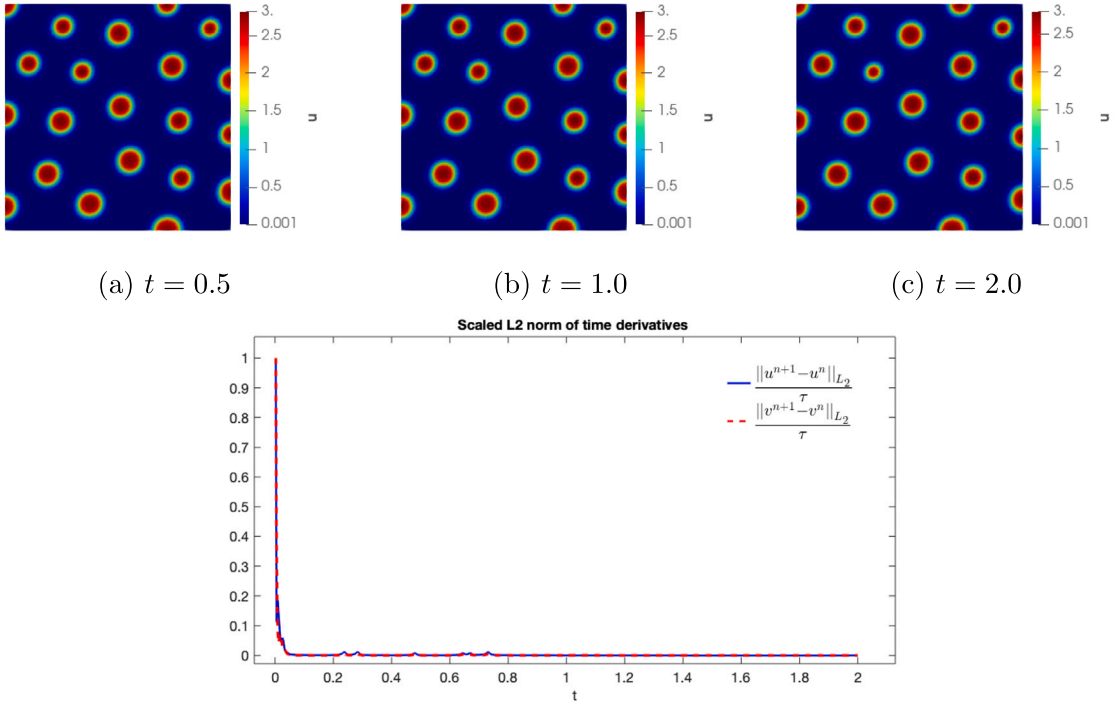

Fig. 12. (a)–(c) Finite element simulations corresponding to the u-component of the reaction–diffusion system (1) with linear cross-diffusion. Model parameter values are selected to satisfy Turing diffusion driven instability conditions as in Theorems 2 and 4, with $d = 16.5$, $\gamma = 340$, $d_u = 4$, $d_v = 4$, $\alpha = 0.075$ and $\beta = 0.3$. (d) Plot of the L_2 norms of the discrete time-derivatives of the solutions u and v. The norms decay rapidly, with the model system converging to a spatially inhomogeneous solution stable over time.

the cross-diffusive system is limited to Turing type only. Fig. 12(a)–(c) indicates the numerical simulations at certain time levels showing the agreement with the conditions presented by Theorems 2 and 4. The convergence in the L_2 norm is presented in Fig. 12(d). The model system exhibits spatially inhomogeneous spot patterns, with smaller radii.

Fig. 13 shows Turing type of instability satisfying the conditions in Theorems 1 and 4 for a different set of parameters. The evolving profile of the component u can be well-captured in Fig. 13(a)–(f), starting with spatially inhomogeneous stripe patterns which evolved with time to spatially inhomogeneous spot patterns, with a relatively large radii. The convergence in the L_2 norm of the successive time steps is observed in Fig. 13(g).

Similarly, Fig. 14 exhibits the Turing type of instability satisfying the conditions in Theorems 1 and 4. The transient solutions from random initial conditions show stripe patterns during the early stages of the formation of the spatially inhomogeneous solution, then, these

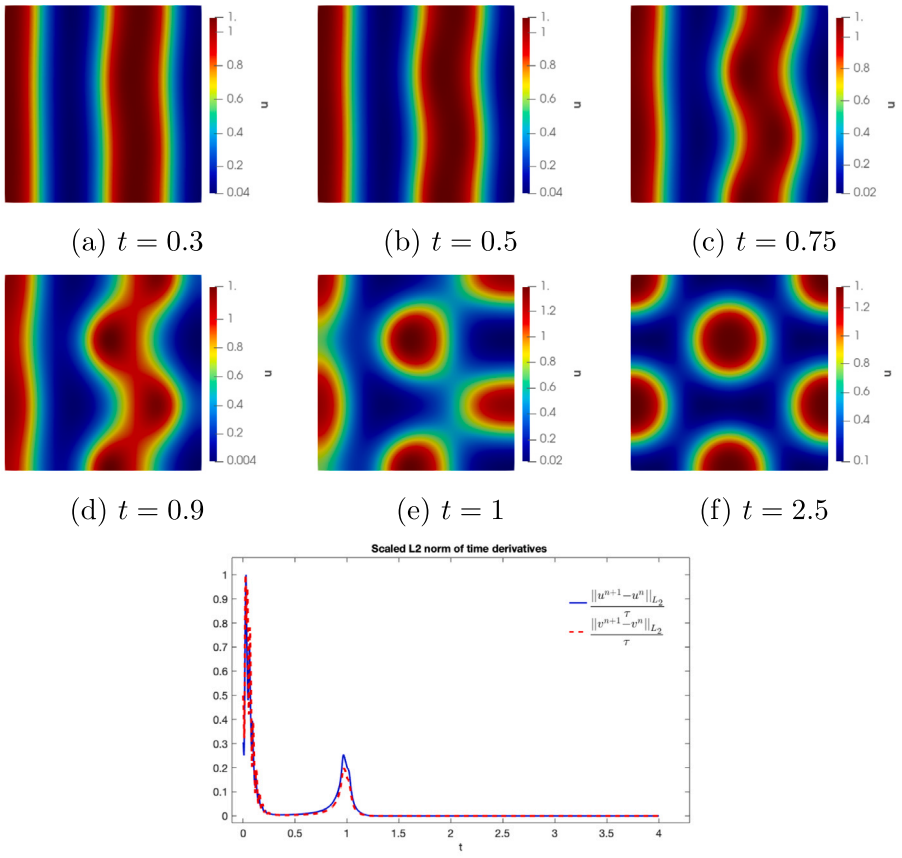

(h) The L_2 norms of the discrete time-derivatives of the solutions u and v

Fig. 13. (a)–(f) Finite element simulations corresponding to the u-component of the reaction–diffusion system (1) with linear cross-diffusion. Model parameter values parameters are chosen to satisfy Turing's diffusion-driven instability conditions as Theorems 1 and 4, with $d = 2.8$, $\gamma = 310$, $d_u = 0.001$, $d_v = 0.41$, $\alpha = 0.025$ and $\beta = 0.55$. (h) Plot of the L_2 norms of the discrete time-derivatives of the solutions u and v. The plot exhibits the three phases described earlier, rapid decay due to the effects of diffusion, followed by exponential growth due to the positivity of the real part of the eigenvalues for the excitable wave numbers and lastly rapid decay leading the model system to converge to a spatially inhomogeneous solution stable over time.

transform into spatially inhomogeneous spot patterns with very large radii.

Fig. 15 presents the spatial pattern formation for the parameters selected from the Turing instability region, particularly to see the effect of negative cross-diffusion as well as $d = 1$. It has been shown in [7] that, in the absence of the cross-diffusion, selection of the main diffusion coefficient as $d = 1$, cannot produce any kind of patterns. In this particular experiment, we observe the spot type patterns and the system is uniformly converging to inhomogeneous solution confirming the theoretical predictions given by Theorems 1 and 4.

In Fig. 16, we confirm that the effect of the choice of model parameters on the formation of spatial patterns is not limited only to spatially inhomogeneous, time-independent patterns but that spatially periodic time-dependent spot patterns can be obtained with large radii. For illustrative purposes, we carry out simulations using the parameters from the Hopf/transcritical region. In each case, the L_2 norms of the discrete time derivatives show the temporal periodical behaviour as predicted by Theorems 1 and 4.

In the conditions stated by Theorems 1, 2, and 4, the eigenmodes m and n appear in the numerator of the rational expressions on the right-hand side of the inequalities. This implies that increasing the values of m and n requires a larger domain size to demonstrate spatiotemporal dynamics, which comes at a significant computational cost. In all simulations shown in Figs. 5–16, we have chosen the domain-size parameter as $L = 1$. For illustration, we have included a simulation shown in Fig. 17 for modes higher than the first excitable wavenumber to demonstrate the robustness of our results. We select model parameters as $d = 1$, $\gamma = 100$, $d_u = d_v = 0.1$, $\alpha = 0.5$ and $\beta = 1.5$ with the domain-size parameter as $L = 10$. We observe that on this large domain size (ten times the unit square), spot-patterns form that have much smaller radii. It is evident that taking larger and large domain size, the spot patterns will become so small that a spatially homogeneous solution will start to emerge. Hence, for very large domains, the ability of the reaction–diffusion system to form patterns is greatly reduced. This is consistent with previous findings by Turing and Murray [1,9].

5. Conclusion

Reaction–diffusion systems with cross-diffusion play a pivotal in the area of pattern formation and are applied in many physical problems in cellular and developmental biology as well as to problems in material and plant sciences. Understanding the role of domain size is crucial in understanding the spatiotemporal behaviour of solutions under different regimes of the parameters. In this study, we have extended substantially our previous analysis of reaction–diffusion systems to study simultaneously domain-size and the presence of linear cross-diffusion, where we have analytically quantified and computed parameter spaces under Turing diffusion-driven instability as well as characterising spaces associated with Hopf and transcritical bifurcations. Conditions for the system to exhibit instability of the uniform steady state (Turing or otherwise) are analytically derived, these ensure that the reaction–diffusion system with linear cross-diffusion gives rise to either time-independent spatially inhomogeneous solutions (a spatial pattern) or time-dependent period solutions (spatial patterning that is

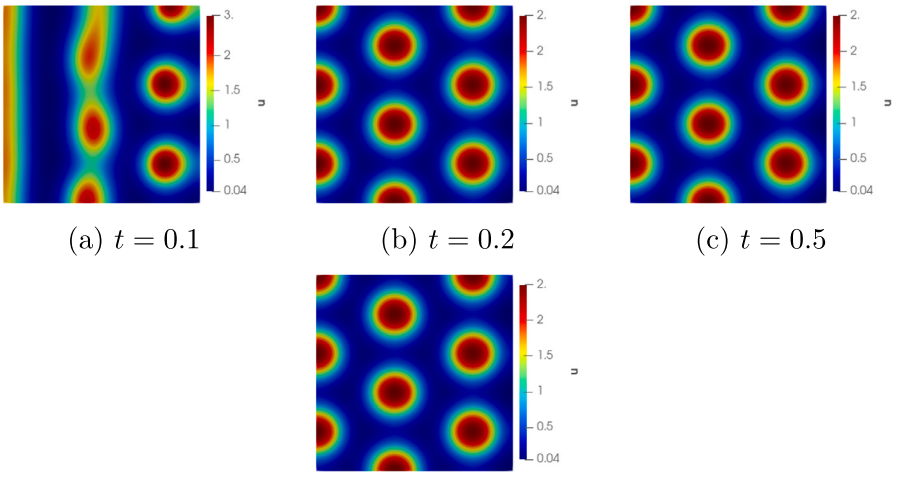

(a) $t = 0.1$ (b) $t = 0.2$ (c) $t = 0.5$

(d) $t = 1.0$

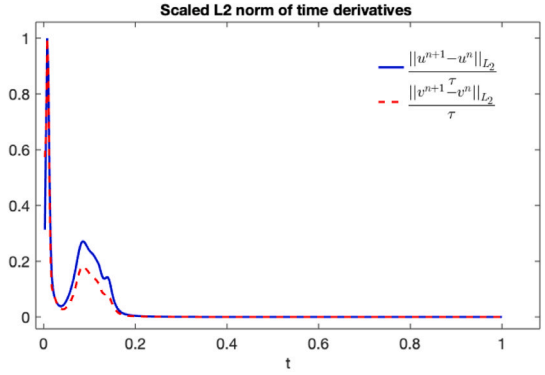

(e) The L_2 norms of the discrete time-derivatives of the solutions u and v

Fig. 14. (a)–(d) Finite element simulations corresponding to the u-component of the reaction–diffusion system (1) with linear cross-diffusion. Model parameter values are chosen to satisfy Turing's diffusion-driven instability conditions as Theorems 1 and 4, with $d = 10$, $\gamma = 750$, $d_u = 0.001$, $d_v = 0.5$, $\alpha = 0.02$ and $\beta = 0.75$. (e) Plot of the L_2 norms of the discrete time-derivatives of the solutions u and v. Similarly, the plot exhibits the three phases described earlier, rapid decay due to the effects of diffusion, followed by exponential growth due to the positivity of the real part of the eigenvalues for the excitable wave numbers and lastly rapid decay leading the model system to converge to a spatially inhomogeneous solution stable over time.

periodic in time). These conditions for pattern formation relate the domain size and system parameters. Parameter spaces of the model system are computed through the use of linear stability theory, close to bifurcation points. To support theoretical findings, appropriate choices of model parameters were determined (from the computed parameter spaces) and used in the finite element numerical method to compute approximate numerical solutions to the reaction–diffusion system with linear cross-diffusion. Finite element solutions exhibit Turing and Hopf/transcritical spatially inhomogeneous time-independent (for the case of Turing patterns) and time-periodic patterns (for Hopf and transcritical).

To demonstrate the role of cross-diffusion in the formation of patterns, as a mechanism for pattern formation, we generated parameter spaces that are only induced by cross-diffusion. For example, in the absence of cross-diffusion, it is well-known in the theory of Turing diffusion-driven instability that the diffusion coefficients of the activator and the inhibitor must differ substantially. In particular, the classical paradigm for pattern formation involves long-range inhibition and short-range activation, which entails that the diffusion coefficient of the inhibitor must be a lot larger compared to the diffusion coefficient of the activator [1,9]. This widely accepted key necessary condition for Turing-type patterning can be relaxed or violated by simply taking equal diffusion coefficients. Under this assumption or restriction, cross-diffusion becomes a dominant factor in driving instability or symmetry breaking of the spatially homogeneous solution, giving rise to the formation of spatial structure. Now, coupling cross-diffusion and the domain size, we generate cross-diffusion induced parameter spaces by taking the non-dimensional diffusion coefficient $d = 1$, where $d = \frac{D_v}{D_u}$, with D_u and D_v the dimensional diffusion coefficients of the activator and inhibitor respectively. Furthermore, we demonstrate the ability of cross-diffusion to induce patterns by generating parameter spaces for positive and negative cross-diffusion coefficients. The only restriction enforced on the diffusion coefficients is the positivity of the determinant of the full diffusion tensor matrix, i.e. $d - d_u d_v > 0$. Also the values of the cross-diffusion coefficients must be selected to ensure the well-posedness of the semi-linear parabolic partial differential system [8,11]. These parameter spaces do not exist in the absence of cross-diffusion, hence the importance of cross-diffusion as a candidate mechanism for pattern generation.

Our theoretical findings when pattern formation is induced by cross-diffusion are then supported by finite element simulations. We exhibit cross-diffusion induced: (i) spatially inhomogeneous patterns (time-independent), (ii) time-dependent constant-amplitude periodic spatially inhomogeneous patterns and (iii) time-dependent non-constant amplitude periodic spatially inhomogeneous patterns. The time-dependency and time-periodicity are illustrated by computing and plotting the discrete L_2 norm measure of the discrete time-derivative. Hence, numerical experiments confirm the existence of pattern formation that can only be possible as a result of and driven by cross-diffusion.

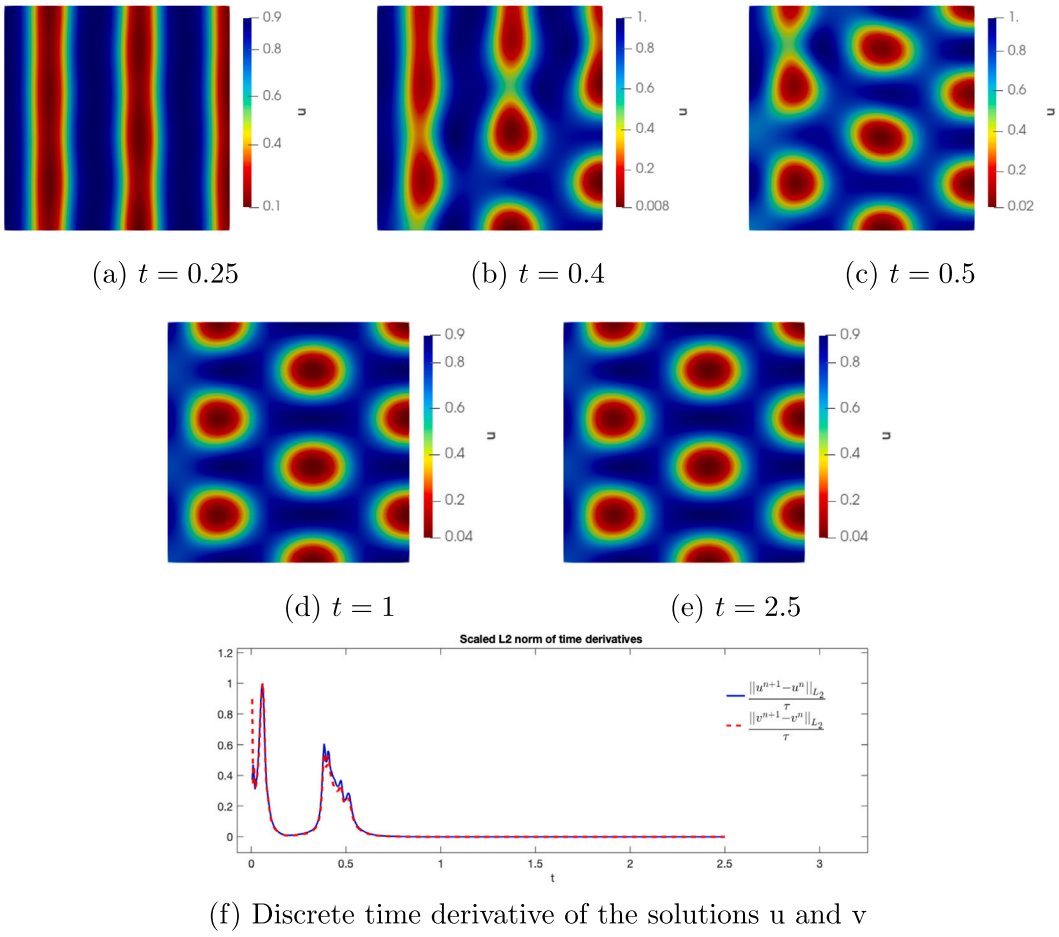

Fig. 15. (a)–(e) Finite element simulations corresponding to the u-component of the reaction–diffusion system (1) with negative cross-diffusion. Model parameter values are chosen to satisfy Turing's diffusion-driven instability conditions as Theorems 1 and 4, with $d = 1$, $\gamma = 500$, $d_u = -0.1$, $d_v = 0.41$, $\alpha = 0.02$ and $\beta = 0.6$. (f) Plot of the L_2 norms of the discrete time-derivatives of the solutions u and v.

Our work so far has been restricted to understanding the role of domain size and parameters when studying the mechanism for symmetry breaking of a reaction–diffusion system in the presence of linear cross-diffusion on stationary rectangular domains. Natural extensions of our work involve the following open problems:

- Understanding the role of domain-size during growth development for reaction–diffusion systems with linear cross-diffusion
- What is the role of nonlinear cross-diffusion as a mechanism for pattern formation? In this case, weakly nonlinear bifurcation analysis must be a candidate technique for analytical purposes.

CRediT authorship contribution statement

Wakil Sarfaraz: Writing – original draft, Visualisation, Validation, Supervision, Methodology, Investigation, Formal analysis, Data curation, Conceptualization. **Gulsemay Yigit:** Writing – original draft, Visualisation, Validation, Software, Methodology, Formal analysis, Data curation. **Raquel Barreira:** Writing – review & editing, Visualization, Validation, Software, Methodology, Investigation. **Lakhdar Remaki:** Writing – review & editing, Validation, Formal analysis. **Muflih Alhazmi:** Writing – review & editing, Formal analysis. **Anotida Madzvamuse:** Writing – review & editing, Visualization, Validation, Supervision, Project administration, Methodology, Investigation, Funding acquisition, Formal analysis, Conceptualization.

Declaration of competing interest

All authors declare that they have no conflict of interest.

Data availability

No data was used for the research described in the article.

Acknowledgements

AM is a Canada Research Chair (Tier 1) in Theoretical and Computational Biology (CRC-2022-00147). This work (AM) was partially supported by the Natural Sciences and Engineering Research Council of Canada (NSERC), Canada, Discovery Grants Program (RGPIN-2023-05231), the British Columbia Foundation for Non-Animal Research and the Engineering, Canada and Physical Sciences Research Council, United Kingdom (EPSRC: EP/J016780/1). AM acknowledges the Royal Society Merit Award (2016–2021) funded generously by the Wolfson Foundation. This work (AM, GY, RB) was partly carried out while AM, GY and RB were at the International Center for Mathematical Sciences (ICMS) in Edinburgh for the Research in Group Meeting (1st–10th September 2022). RB was partly supported by National Funding from FCT - Fundação para a Ciência e a Tecnologia, Portugal, under the project UIDB/04561/2020. WS acknowledges the support from UBC Mathematics Department, Canada, start-up fund grant (awarded to AM) for open-source publication costs of the article.

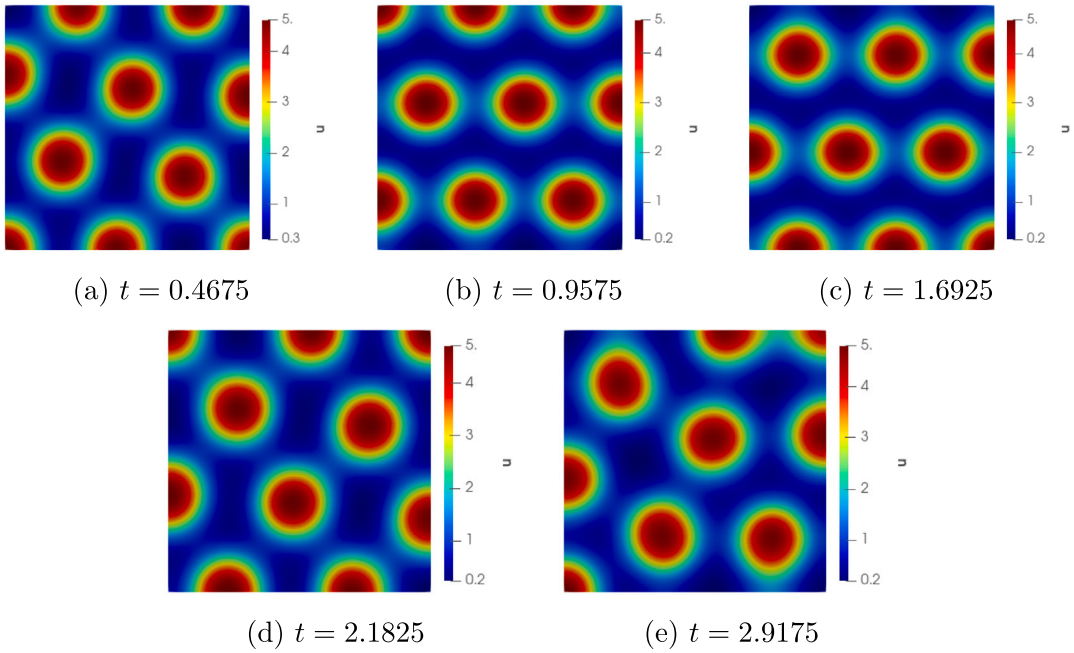

(f) The L_2 norms of the discrete time-derivatives of the solutions u and v

Fig. 16. (a)–(e) Finite element simulations corresponding to the u-component of the reaction–diffusion system (1) with linear cross-diffusion. Model parameter values are selected to satisfy Hopf/Transcritical bifurcation given in Theorems 1 and 4, with $d = 7$, $\gamma = 150$, $d_u = 0.01$, $d_v = 2.5$, $\alpha = 0.075$ and $\beta = 0.15$. (f) Plot of the L_2 norm of the discrete time-derivative of the solutions u and v. The L_2 norms behave differently, these exhibit unequal amplitudes at regular periodic time. The time-evolution of the spatially inhomogeneous solutions appears to alternate between regular horizontally oriented spot patterns and zigzag oriented spot patterns. This could be due to re-orientation in patterns during transitions from spatially uniform homogeneous steady states to spatially inhomogeneous solutions. However, the number of spots remain relatively constant.

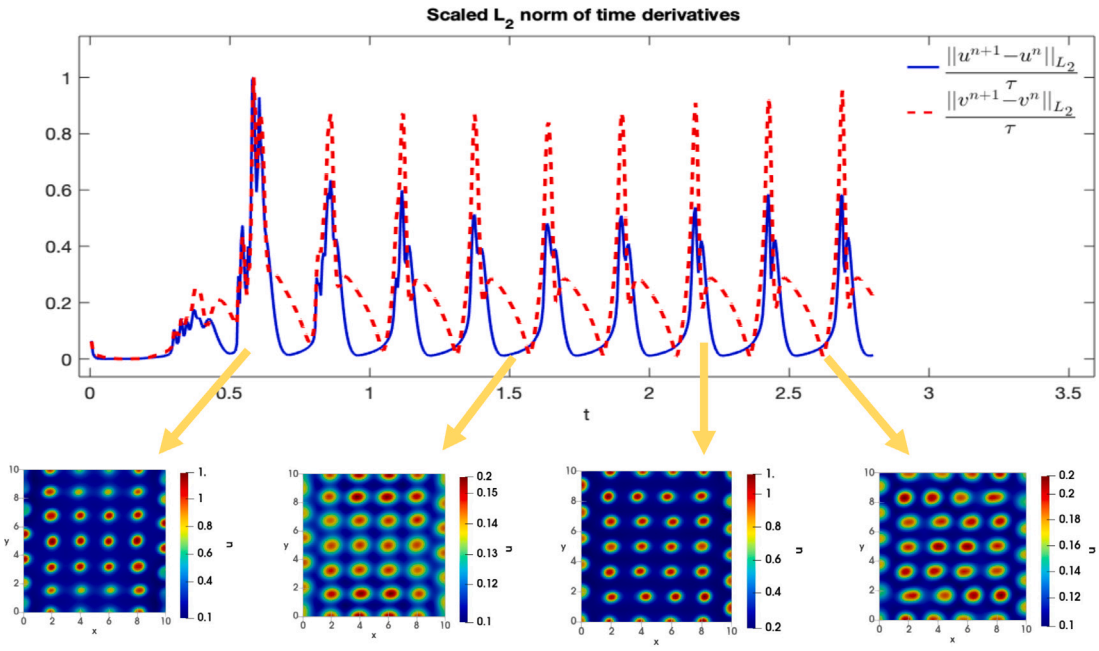

Fig. 17. Finite element simulations corresponding to the u-component of the reaction–diffusion system (1) with linear cross-diffusion. Parameter values are selected to satisfy conditions (17) and (24) of Theorems 1 and 4, respectively, with $L = 10$, $d = 1$, $\gamma = 155$, $d_u = 0.01$, $d_v = 0.55$, $\alpha = 0.085$ and $\beta = 0.1$.

References

[1] Murray JD. Mathematical biology II: Spatial models and biomedical applications, vol. 3, Springer New York; 2001.

[2] Madzvamuse A. A numerical approach to the study of spatial pattern formation (Ph.D. thesis), University of Oxford; 2000.

[3] Gierer A, Meinhardt H. A theory of biological pattern formation. Kybernetic 1972;12:30–9.

[4] Vanag VK, Epstein IR. Cross-diffusion and pattern formation in reaction–diffusion systems. Phys Chem Chem Phys 2009;11(6):897–912.

[5] Vanag VK, Epstein IR. Pattern formation mechanisms in reaction-diffusion systems. Int J Dev Biol 2009;53(5–6):673–81.

[6] Madzvamuse A, Gaffney EA, Maini PK. Stability analysis of non-autonomous reaction-diffusion systems: the effects of growing domains. J Math Biol 2010;61:133–64.

[7] Madzvamuse A, Ndakwo HS, Barreira R. Cross-diffusion-driven instability for reaction-diffusion systems: analysis and simulations. J Math Biol 2015;70(4):709–43.

[8] Madzvamuse A, Ndakwo H, Barreira R. Stability analysis of reaction-diffusion models on evolving domains: the effects of cross-diffusion. Discrete Contin Dyn Syst 2015;36(4):2133–70.

[9] Turing AM. The chemical basis of morphogenesis. Bull Math Biol 1990;52(1–2):153–97.

[10] Schnakenberg J. Simple chemical reaction systems with limit cycle behaviour. J Theoret Biol 1979;81(3):389–400.

[11] Madzvamuse A, Barreira R. Domain-growth-induced patterning for reaction-diffusion systems with linear cross-diffusion. Discrete Contin Dyn Syst Ser B 2018;23(7):2775–801.

[12] McAfee MS, Annunziata O. Cross-diffusion in a colloid–polymer aqueous system. Fluid Phase Equilib 2013;356:46–55.

[13] Barrios EC, Krause TC, Annunziata O. Salt-induced diffusiophoresis of a nonionic micelle: Roles of salting out and proximity to surfactant cloud point. J Mol Liq 2022;359:119271.

[14] Tang X, Song Y. Cross-diffusion induced spatiotemporal patterns in a predator–prey model with herd behavior. Nonlinear Anal Real World Appl 2015;24:36–49.

[15] Li Q, Liu Z, Yuan S. Cross-diffusion induced Turing instability for a competition model with saturation effect. Appl Math Comput 2019;347:64–77.

[16] Gambino G, Lombardo M, Sammartino M. Cross-diffusion-induced subharmonic spatial resonances in a predator-prey system. Phys Rev E 2018;97(1):012220.

[17] Medvinsky AB, Petrovskii SV, Tikhonova IA, Malchow H, Li B-L. Spatiotemporal complexity of plankton and fish dynamics. SIAM Rev 2002;44(3):311–70.

[18] Leyva JF, Málaga C, Plaza RG. The effects of nutrient chemotaxis on bacterial aggregation patterns with non-linear degenerate cross diffusion. Phys A 2013;392(22):5644–62.

[19] Zemskov EP, Vanag VK, Epstein IR. Amplitude equations for reaction-diffusion systems with cross diffusion. Phys Rev E 2011;84(3):036216.

[20] Mackenzie J, Madzvamuse A. Analysis of stability and convergence of finite-difference methods for a reaction–diffusion problem on a one-dimensional growing domain. IMA J Numer Anal 2011;31(1):212–32.

[21] Madzvamuse A, Chung AH, Venkataraman C. Stability analysis and simulations of coupled bulk-surface reaction–diffusion systems. Proc R Soc A 2015;471(2175):20140546.

[22] Sarfaraz W, Madzvamuse A. Classification of parameter spaces for a reaction-diffusion model on stationary domains. Chaos Solitons Fractals 2017;103:33–51.

[23] Woolley TE, Krause AL, Gaffney EA. Bespoke turing systems. Bull Math Biol 2021;83:1–32.

[24] Sarfaraz W, Madzvamuse A. Domain-dependent stability analysis of a reaction–diffusion model on compact circular geometries. Int J Bifurcation Chaos 2018;28(08):1830024.

[25] Sarfaraz W, Madzvamuse A. Stability analysis and parameter classification of a reaction–diffusion model on an annulus. J Appl Nonlinear Dyn 2020;9(4):589–617.

[26] Xu C, Wei J. Hopf bifurcation analysis in a one-dimensional Schnakenberg reaction–diffusion model. Nonlinear Anal Real World Appl 2012;13(4):1961–77.

[27] Liu P, Shi J, Wang Y, Feng X. Bifurcation analysis of reaction–diffusion Schnakenberg model. J Math Chem 2013;51(8):2001–19.

[28] Gaffney E, Yi F, Lee S. The bifurcation analysis of Turing pattern formation induced by delay and diffusion in the Schnakenberg system. Discrete Contin Dyn Syst-Ser B 2016;22(2).

[29] Yi F. Turing instability of the periodic solutions for reaction-diffusion systems with cross-diffusion and the patch model with cross-diffusion-like coupling. J Differential Equations 2021;281:379–410.

[30] Jiang W, Wang H, Cao X. Turing instability and Turing–Hopf bifurcation in diffusive Schnakenberg systems with gene expression time delay. J Dynam Differential Equations 2019;31:2223–47.

[31] Bilazeroğlu Ş, Merdan H. Hopf bifurcations in a class of reaction-diffusion equations including two discrete time delays: An algorithm for determining Hopf bifurcation, and its applications. Chaos Solitons Fractals 2021;142:110391.

[32] Alfifi H. Stability analysis for Schnakenberg reaction-diffusion model with gene expression time delay. Chaos Solitons Fractals 2022;155:111730.

[33] Zhang J-F, Shi H-B, Madzvamuse A. Characterizing the effects of self-and cross-diffusion on stationary patterns of a Predator–Prey system. Int J Bifurcation Chaos 2020;30(03):2050041.

[34] Wu S, Song Y. Spatiotemporal dynamics of a diffusive predator-prey model with nonlocal effect and delay. Commun Nonlinear Sci Numer Simul 2020;89:105310.

[35] Cao J, Sun H, Hao P, Wang P. Bifurcation and turing instability for a predator-prey model with nonlinear reaction cross-diffusion. Appl Math Model 2021;89:1663–77.

[36] Liu Y, Duan D, Niu B. Spatiotemporal dynamics in a diffusive predator–prey model with group defense and nonlocal competition. Appl Math Lett 2020;103:106175.

[37] Yigit G, Sarfaraz W, Barreira R, Madzvamuse A. A domain-dependent stability analysis of reaction–diffusion systems with linear cross-diffusion on circular domains. Nonlinear Anal Real World Appl 2024;77:104042.
[38] Aymard B. On pattern formation in reaction–diffusion systems containing self-and cross-diffusion. Commun Nonlinear Sci Numer Simul 2022;105:106090.
[39] Madzvamuse A, Maini PK. Velocity-induced numerical solutions of reaction-diffusion systems on continuously growing domains. J Comput Phys 2007;225(1):100–19.
[40] Barreira R, Elliott CM, Madzvamuse A. The surface finite element method for pattern formation on evolving biological surfaces. J Math Biol 2011;63:1095–119.
[41] Lakkis O, Madzvamuse A, Venkataraman C. Implicit–explicit timestepping with finite element approximation of reaction–diffusion systems on evolving domains. SIAM J Numer Anal 2013;51(4):2309–30.
[42] Madzvamuse A, Chung AH. Fully implicit time-stepping schemes and non-linear solvers for systems of reaction–diffusion equations. Appl Math Comput 2014;244:361–74.
[43] Tuncer N, Madzvamuse A. Projected finite elements for systems of reaction-diffusion equations on closed evolving spheroidal surfaces. Commun Comput Phys 2017;21(3):718–47.
[44] Madzvamuse A. Time-stepping schemes for moving grid finite elements applied to reaction–diffusion systems on fixed and growing domains. J Comput Phys 2006;214(1):239–63.
[45] Evans LC. Partial differential equations, vol. 19, American Mathematical Society; 2022.
[46] Ockendon JR. Applied partial differential equations. Oxford University Press; 2003.
[47] Smoller J. Shock waves and reaction—diffusion equations, vol. 258, Springer Science & Business Media; 2012.
[48] Venkataraman C, Lakkis O, Madzvamuse A. Global existence for semilinear reaction–diffusion systems on evolving domains. J Math Biol 2012;64:41–67.
[49] Schmidt JW, Heß W. Positivity of cubic polynomials on intervals and positive spline interpolation. BIT Numer Math 1988;28:340–52.
[50] Qi L, Song Y, Zhang X. Positivity conditions for cubic, quartic and quintic polynomials. 2020, arXiv preprint arXiv:2008.10922.
[51] Madzvamuse A, Barreira R. Exhibiting cross-diffusion-induced patterns for reaction-diffusion systems on evolving domains and surfaces. Phys Rev E 2014;90(4):043307.
[52] Madzvamuse A. A modified backward Euler scheme for advection-reaction-diffusion systems. In: Mathematical modeling of biological systems, volume i: Cellular biophysics, regulatory networks, development, biomedicine, and data analysis. Springer; 2007, p. 183–9.